ENGINEERING RESEARCH INSTITUTE
UNIVERSITY OF MICHIGAN
ANN ARBOR

QUARTERLY PROGRESS REPORT NO. 3

AN INVESTIGATION OF INTERGRANULAR OXIDATION IN STAINLESS STEEL

By

C. A. SIEBERT

M. J. SINNOTT

R. E. KEITH

Project 2110

DEPARTMENT OF THE AIR FORCE, WRIGHT AIR DEVELOPMENT CENTER
WRIGHT-PATTERSON AIR FORCE BASE
CONTRACT AF 33(616)-353

September, 1953

QUARTERLY PROGRESS REPORT NO. 3

AN INVESTIGATION OF INTERGRANULAR OXIDATION IN STAINLESS STEEL

INTRODUCTION

This research project has been undertaken under the sponsorship of the Wright Air Development Center of the U. S. Air Force. Its objectives are fourfold:

(a) to determine the effect of temperatures between 1600 and 2000°F on intergranular oxidation or corrosion;

(b) to examine the effects of alloy composition on intergranular oxidation or corrosion;

(c) to determine the nature of the penetrating material in areas of intergranular attack; and

(d) to devise methods of reducing or eliminating intergranular penetration.

MATERIAL

All work during the past quarter has been carried out using sheet material of three different analyses and having thicknesses in the range 0.05-0.07 inch. These alloys were provided by the General Electric Company.

One of the materials is basically type 309 stainless steel with a niobium addition, and the other two are different heats of type 310 stainless steel. Chemical analyses are presented in Table I.

TABLE I

COMPOSITION OF STAINLESS-STEEL STOCK, WEIGHT PERCENT

Alloy	C	Ni	Cr	Si	Mn	P	S	Mo	Cu	Co	W	Nb
309 + Nb	0.08	15.39	22.64	0.46	2.31	0.012	0.008	*	*	*	*	0.82
310												
Ht. 64177	0.13	16.96	24.03	0.55	0.42	0.018	0.008	0.033	0.13	0.01	<0.01	*
Ht. 64270	0.12	19.14	22.30	0.43	0.50	0.025	0.008	0.042	0.10	0.01	<0.01	*

*No analysis

PROCEDURE

Specimen Preparation

Rectangular specimens 1/2 by 1 inch are first cut from the stock by means of a band saw. A record is kept of the location of each specimen in the stock. The edges are smoothed and rounded on a grinding wheel. The specimens are marked with a small punch impression on the side that is to face downward in the furnace, cleaned with acetone, and placed in holders as shown in Fig. 1. These holders are made from ceramic combustion carbon-analysis boats with their covers cemented in an inverted position. This type of holder was adopted in preference to the wire frames previously used for two reasons: first, difficulty was encountered in quenching the thin specimens, which tended to adhere to the wire frames; and, second, there was considerable contamination of the collected oxide with oxide from the wires. The use of ceramic boats solved both these problems. By marking the bottom sides of the specimens, effects arising from air flow restrictions on the bottom side, if any, can be taken into account.

Test Procedure

The specimen holders are charged into the battery of the four tube furnaces described in detail in the last progress report[1]. These four furnaces

[1]C. A. Siebert, M. J. Sinnott, R. E. Keith, Quarterly Progress Report No. 2, An Investigation of Intergranular Oxidation in Stainless Steel, Wright Air Development Center, U. S. Air Force, Contract Af 33(616)-353, June, 1953.

are operated at temperatures of 1600, 1700, 1800, and 1900°F respectively. Furnaces are on temperature and are purged with air of the required humidity and at the required velocity before specimens are charged. One specimen of each of the three alloys is charged to each furnace. Position of the specimen of a particular alloy in the furnace is randomized both from furnace to furnace and from run to run; thus any small variations in temperature distributions will have a minimum effect on the results. During the run, furnace temperatures and air flow rates are measured twice a day, and the dew point of the air is measured once a day.

End-of-Run Procedure. At the conclusion of the oxidation period, the specimens are quenched and the free oxide from each specimen is collected by filtration of the distilled-water quenching medium. The oxide is then dried in acetone and ether and is bottled. It is examined visually and tested with a magnet. The oxide is then pulverized and X-ray powder specimens are made from it.

The oxidized metal specimens are examined visually. A small strip is then sawed off each specimen parallel to the long dimension and is discarded. The purpose of this is to insure freedom from edge effects in the subsequent examination. A 90° bend is then made in each specimen perpendicular to the cut edge. This operation is carried out in a small arbor press, using a die constructed for the purpose, shown in Fig. 2. The specimens thus stand by themselves, which simplifies the problem of mounting for metallographic examination and assures a true thickness measurement. At this point, a magnetic examination is made. A specimen is balanced on the bent portion and a magnet is brought repeatedly near one of the upturned straight sections. The test is surprisingly sensitive, some specimens showing quite strong surface magnetism.

Penetration Measurements

The bent specimens are next mounted in bakelite. There are five specimens per mount: the four specimens of a particular alloy which have been oxidized and a fifth specimen cut from the same area of the stock but not oxidized. The purpose of the control specimen is to provide a measurement of the unoxidized, or original, specimen thickness.

After the specimens have been mounted, they are given a metallographic polish but are not etched. For making penetration measurements on the polished specimens, a metallurgical microscope equipped with a 4-mm objective lens, a micrometer stage, and a Bausch and Lomb grain-size eyepiece is used. The surface of a specimen cross section is aligned with one edge of the A.S.T.M. No. 6 grid of the eyepiece, and the entire straight portion of the surface is traversed. The number of intergranular fissures ending in

each row of the grid is recorded, and the figures thus obtained are divided by the total length traversed (which runs from 1.1 to 1.3 inches) to put them on a comparative basis. The size of the squares of the eyepiece grid has been determined by calibration with a stage micrometer. Thus at least an approximation can be obtained to the true curve relating distance from the surface to the number of fissures having that depth for each specimen. Curves obtained by this method appear in Figs. 3 through 17. This method of measuring penetration, though tedious, is subject to less chance of error than any other practical method that we have been able to devise, although it could be wished that even this method were less subject to human errors caused by misinterpretation and operator fatigue.

Thickness Measurements

Thickness measurements can be made, to a degree of precision limited only by the roughness of the individual specimens, by use of the travelling stage of a Tukon hardness tester.

Metallographic Examination

In addition to the microscope examination accompanying the penetration measurements, each specimen is examined in detail at 1000 diameters on a Bausch and Lomb research metallograph under both bright-field and polarized light, a record being made of the nature of the penetration and the location of suitable areas for photomicrographs. Examinations have also been made using dark-field illumination, but were unfruitful.

Punch Card File

A punch card file is being made, the data from each specimen being summarized on a single card. It is hoped that this file will save a considerable amount of time in the analysis of results.

EQUIPMENT

Argon-Oxygen Furnace

In addition to the four tube furnaces and associated equipment for the control of air flow described in detail in Progress Report No. 2, a furnace of similar construction has been prepared for use with atmospheres of

argon and very small percentages of oxygen. Any residual oxygen and most of any residual nitrogen are removed from the bottled argon by passing it over titanium chips at a temperature of approximately 1800°F. The argon is then cooled and metered, and sufficient bottled oxygen is blended with it to produce controlled mixtures of the order of 1 percent or less of oxygen. The gas is then introduced into the furnace. The purpose of using this type of atmosphere is to obtain some specimens having extremely severe intergranular penetration without the surface oxidation usually occurring. These specimens will be used in determining the composition of the intergranular penetrating material.

Phosphorus Pentoxide Dryer

Considerable difficulty has been encountered in maintaining low air humidity throughout a run in the original equipment using a dryer containing activated alumina. The difficulty seems to lie in inadequate methods for regeneration. Furthermore, even the lowest dewpoints obtainable with alumina are not as low as might be desired. Therefore, a vessel is being constructed which is intended to hold phosphorus pentoxide. This dryer will be used in conjunction with the alumina dryer.

Humidifier

In order to obtain dewpoints above +20°F, a small humidifying tower is being designed.

RESULTS AND DISCUSSION

Thickness Measurements

Measurements of specimen thickness were made for one run (Run 5), and it was found that there is no significant change in cross section accompanying 100 hours of oxidation at temperatures between 1600 and 1900°F and a dewpoint of less than -20°F. There was more variability of thickness along the sheets of stock than there was variability due to oxidation. It can be stated that any change in specimen thickness under the above oxidation conditions is certainly less than 0.0001 inch in all three of the materials tested. No further thickness measurements have been made up to the present time, since thickness measurements were considered to be of less importance than penetration measurements in this investigation. All penetration measurements must therefore be reported as penetration relative to the metal-oxide interface, rather than as penetration relative to the original metal surface.

X-Ray Diffraction Studies

As was mentioned in the Procedure section, X-ray powder diffraction photographs are being taken of the oxide scales. The purpose of this phase of the investigation is twofold. First, it is desirable to know the composition of the scale in order to determine whether there is any significant difference between it and the material in the intergranular fissures. Second, it is hoped that resistance to intergranular penetration may be associated with the formation of a protective oxide layer of unique composition on the surface of the metal.

Two series of four X-ray photographs have been made on a Debye-Scherrer camera of 11.4-cm diameter using filtered chromium K radiation. The specimens selected for this work were the oxides from the Type 309 alloy and Heat 64177 of the type 310 alloy. The specimens are the oxides resulting from oxidation at 1600, 1700, 1800, and 1900°F and are from Run 5. The diffraction patterns from both alloys are quite complex. The patterns were checked for the presence of the more obvious oxides as soon as they were obtained. These oxides included: FeO, Fe_2O_3, Fe_3O_4, $Fe_2O_3 \cdot NiO$, $2FeO \cdot SiO_2$, $Cr_2O_3 \cdot FeO$, $Cr_2O_3 \cdot Fe_2O_3$, $3Cr_2O_3 \cdot Fe_2O_3$, $Cr_2O_3 \cdot 3Fe_2O_3$, Cr_2O_3, $Cr_2O_3 \cdot NiO$, $NiO \cdot SiO_2$ in the forms of cristobalite and quartz, $2MnO \cdot SiO_2$, MnO, Mn_2O_3, Mn_3O_4, and the five forms of Al_2O_3 appearing in the A.S.T.M. card index. In addition, the patterns were checked for the presence of the metals Fe, Ni, Cr, and Mn.

The only definite identifications that have been made to date are of Cr_2O_3, Fe_3O_4, and NiO in the type 309 oxides, and Cr_2O_3, Fe_2O_3, and NiO in the type 310 oxides. These compounds account for only 18 of the 50 lines observed in the type 309 oxides and 18 of the 42 lines observed in the type 310 oxides. The method of analysis presently being tried consists of observing increases and decreases in the intensities of different groups of lines as the temperature of oxidation is increased. In this way it is hoped that lines belonging to the same compound can be associated properly. Since the quantitative line-intensity data were only recently obtained and have not yet been evaluated, the actual X-ray data will not be reported at this time.

Once the present patterns have been completely analyzed, exposures will be made on a smaller camera, and the intensities of representative strong lines for each compound will be measured and compared in order to obtain a rough quantitative analyses of the scales.

Penetration Measurements

While we do believe that the method of making penetration measurements which was described in detail in the Procedure section is superior to

any other method with which we are acquainted--primarily because of its relatively large sample size--the method is subject to certain limitations in practice. In the first place, there is a certain amount of interpretation which the operator must perform. For example, many fissures join and/or separate as they run deeper into the metal. The rule has been adopted that the fissures are to be counted at their ends. Even so, such structures as the one appearing in Fig. 19a are difficult to count properly. A further measuring difficulty occurs in structures where the fissures appear to be discontinuous, where it is sometimes difficult to locate the ends of individual fissures.

Other factors which are involved in the overall reliability of the penetration measurements include the possibilities of poor polishing and rounding of the edges of the specimen. Not to be overlooked is the factor of operator fatigue. These factors are present to a greater or lesser degree in any observational technique of this type, however, and their effects can be reduced to small proportions as experience is gained by the operator.

It is felt that the penetration data presented in this report are sufficiently accurate to show differences among specimens. It would not be wise, however to draw very many quantitative conclusions from the numbers on the graphs, which are presented in Figs. 3 through 17. These curves show the number of fissures per inch having a given depth as the ordinate and the depth itself as the abcissa, the depth being relative to the metal-oxide interface. The curves were constructed by first plotting the number of fissures in each depth interval as a horizontal line extending over that interval, and then drawing the smooth curve best approximating the horizontal lines. These lines have been included in Fig. 15 as an example, but for the sake of clarity, have not been drawn in the other graphs.

In general, two shapes of curves have been observed. The first type is one in which there is a continually decreasing number of fissures ending at increasing depths. This results in a shape that is commonly referred to as a decay curve. The second type of curve is one in which there is a maximum number of fissures at some particular depth. There are at least three possible explanations for this second type of curve, all three of which are probably valid to a greater or lesser extent:

(1) Increasing roughness of the oxidized surface of the specimen, which does tend to take place at the higher oxidizing temperatures, makes it more difficult to see the smaller fissures.

(2) An operator may allow himself to overlook small fissures when there are many larger fissures in the microscope field.

(3) The effect may be a real one, arising naturally from the growth of a finite number of fissures. If oxidation is continued after

all the available favorable surface locations for the beginning of fissures (fissure "nuclei") are utilized, a maximum in the curve would be expected to develop and travel in the direction of greater depth with increasing time. Thus a curve having a maximum may be a further stage of development of a curve having the shape of a decay curve.

In the light of the foregoing discussion, the penetration data from four runs presented in Figs. 3 through 17 will be discussed in detail. Four additional runs have been made, two of which are considered of little value due to failure of the dryer to maintain a constant dewpoint, and two of which have not yet been measured because of time limitations.

The first phase of the program was designed to show the effect of air velocity through the furnaces. The second phase, coincident with part of the first phase, was intended to investigate qualitatively the effect of prior cold work (bending) on penetration. The third phase, which has not yet been fully evaluated, was concerned with the effect of time. In the following discussion, runs will be taken up in logical, rather than numerical, order.

Run 6 Conditions: Air velocity - 20 ft/min
Duration - 100 hrs
Dewpoint - from -20 to +20°F

The type 309 alloy, penetration curves for which appear in Fig. 3, showed a progressive increase in penetration with increasing temperature, with the development of a maximum in the curve at 1900°F. The type 309 alloy seems always to show greater penetration than the type 310.

Heat 64177 (Fig. 4) showed no significant temperature dependence in this run. It might be mentioned at this point that Heat 64177 has rather severe penetration in the as-received condition. The penetration, typical examples of which are shown in Fig. 18, consists largely of a fine tracery of grain-boundary oxidation running just under the surface. This penetration probably resulted from the hot-rolling operation. The conditions is also accompanied by characteristic outward bursts of grains adjacent to the points on the surface where penetration began. During the oxidation tests, further oxidation takes place in the penetration tracery already present resulting in profound deterioration of the surface layer, as illustrated in Fig. 19 a, b, c, and d for temperatures of 1600°, 1700°, 1800°, and 1900°F. Little further penetration took place during the run because the available oxygen combined before reaching the end of the fissures already present.

Heat 64270, which has no penetration in the as-received condition, showed a little more penetration (Fig. 5) than Heat 64177, but not as much as

the type 309. The shapes of the penetration curves change from the decay type to the type exhibiting a maximum as temperature is increased. Typical photomicrographs of the structures developed are presented in Figs. 20 a, b, c, and d for temperatures of 1600°, 1700°, 1800°, and 1900°F.

Run 9 Conditions: Air velocity - 30 ft/min
Duration - 100 hrs
Dewpoint - -60 to -30°F

The primary purpose of this run was to make a qualitative judgment as to the effect of cold work on penetration. Specimens were given a sharp 90° bend before being charged to the furnaces, and penetration measurements were made on both the straight and curved portions of the finished specimens. The results are presented in Figs. 6 through 11. The measurements on the straight sections can be considered indicative of penetration measurements on as-received material under the conditions of the test.

Type 309 alloy (Fig. 6) showed somewhat more penetration at 1600°F than in Run 6, and the maxima in the curves developed at 1800°F and were somewhat deeper than in Run 6. Typical photomicrographs of the structures developed appear in Fig. 21 a, b, c, and d for temperatures of 1600°, 1700°, 1800°, and 1900°F. There were several areas of an unusual sort of penetration structure occurring at 1900°F in addition to the more normal form. An example of this unusual structure is shown in Fig. 22.

Heat 64177 (Fig. 7) showed about the same amount of penetration as in Run 6, but the shapes of the curves looked as though maxima were in the process of developing.

Heat 64270 (Fig. 8) showed penetration curves that were steeper than in Run 6, there being more shallow penetration. There was correspondingly less deep penetration, however, so that the overall amount of penetration was about the same as in Run 6. There was no observable temperature dependence.

The penetration measurements made on the curved portions of the specimens, Figs. 9 through 11, appear to show less penetration than on the straight sections. It must be remembered, however, that these measurements were made on surfaces which were only about one-third the length of the straight surfaces. In other words, the sample size was smaller. Furthermore, the numbers used for these curved lengths, by which the experimental penetration counts were divided, had to be obtained by difference, assuming that the overall specimen lengths were 1 inch and subtracting the known lengths of the straight sections. It is certain, from the appearance of the specimens, however, that the difference in penetration between the straight and curved sections is very slight, if there is a difference at all. There are apparently

no catastrophic effects induced by prior cold work. These results were expected, since cold work introduced prior to testing would probably have annealed out before appreciable oxidation occurred. The only possible deleterious effect of such cold work might arise from cracking of the material during bending, which is unlikely in previously annealed material.

Run 8 Conditions: Air velocity - 30 ft/min
Duration - 100 hrs
Dewpoint - +20°F

The purpose of this run was to find the effect of as high a dewpoint as possible on penetration. The dewpoint of +20°F is that of the compressed air as it comes from the line. No alumina was in the dryer during the run.

The type 309 alloy (Fig. 12) showed somewhat less overall penetration than either Run 6 or 9. The penetration deepened slightly at 1800 and 1900°F. A peculiar type of penetration was observed in the 1900°F specimen, an example of which is shown in Fig. 23. The entire surface was covered with characteristically smooth elongated globular inclusions penetrating inward, but few had any direct connection with the surface; at least there were few connections in the plane of polish. The inclusion areas are filled with what may be bakelite from the mounting operation. An occasional penetration of this sort has been observed from time to time in a number of other specimens; an example of what is believed to be the same type of penetration occurring at 1800°F was presented in the last progress report.

Heat 64177 (Fig. 13) showed about the same amount of penetration as in Runs 6 and 9, or possibly a little less. The behavior of the shapes of the curves is different from previous runs also, in that it is the specimen oxidized at the highest temperature in which the penetration curve shows no maximum.

Heat 64270 (Fig. 14) showed about the same behavior as Run 9 except at 1900°F, in which specimen the penetration was somewhat less than in Run 9.

Run 5 Conditions: Air velocity - 40 ft/min
Duration - 100 hrs
Dewpoint - -20°F

It should be borne in mind, before attempting to relate the results of this run to the runs previously described, that this run was the first one made using material of 0.05-inch thickness. This was also the first run on which the present technique of making penetration measurements was tried. It is possible that, after the additional experience of reading other specimens, Run 5 would now be read differently. If time permits, this run will be re-examined.

The type 309 alloy (Fig. 15) showed deeper penetration at 1600 and 1700°F than at 1800 and 1900°F with maxima occurring at the former two temperatures. This is opposite to the effects observed in the other runs, but could be explained if it were postulated that the progressive surface oxidation had proceeded at a rate that increased faster with temperature than did the rate of intergranular penetration. Why such a condition should prevail on this run only is not known.

Heat 64177 (Fig. 16) showed essentially identical penetration at 1600 and 1900°F and slightly less at 1700 and 1800°F. All the curves were of the decay type. The amount of penetration was about the same as in Run 6.

Heat 64270 (Fig. 17) showed less penetration than that heat had shown in any other run. Furthermore, the penetration decreased with increasing temperature, which might indicate that there was accelerated surface oxidation. One feature of Fig. 17 which should be mentioned is that a measurement was (inadvertantly) made on the as-received, or control, specimen mounted along with the oxidized specimens. Since Heat 64270 did not have any penetration in the as-received condition, this measurement gives some indication of how much error is likely to have been included in penetration readings at that stage in the experience of the operator.

Visual and Magnetic Examinations

There is a difference in the external scales associated with the type 309 and the type 310 alloys. The former tends to have a thick, flaky, nonadherent gray scale, which may or may not have a dull green substrate. The metal beneath this scale is usually smooth light gray, often with a number of interference colors presumably resulting from thin adherent oxide films. The type 310, on the other hand, tends to develop a more adherent, powdery black or gray-black scale, generally in smaller quantities than the type 309.

The majority of the oxides examined, and particularly those from the type 309, are at least weakly magnetic. Magnetic examinations of the type 310 alloy after testing invariably give negative results. The surface of the Type 309, however, has been found to have become rather strongly magnetic after only 10 hours of oxidation. Judging from the strength of the magnetic attraction, it seems likely that it resulted from alloy depletion of the surface and consequent ferrite formation, rather than from adherent magnetic scale. This tentative conclusion will be checked shortly when examinations of etched specimens are begun.

Mention should be made of the presence of a small number of nonmetallic inclusions throughout the cross sections of all three of the materials in the as-received condition. These particles are gray in color and tend to

be hexagonal in shape, as shown in Fig. 24. They will be more adequately identified when the specimens are etched, but are probably particles of corundum, Al_2O_3.

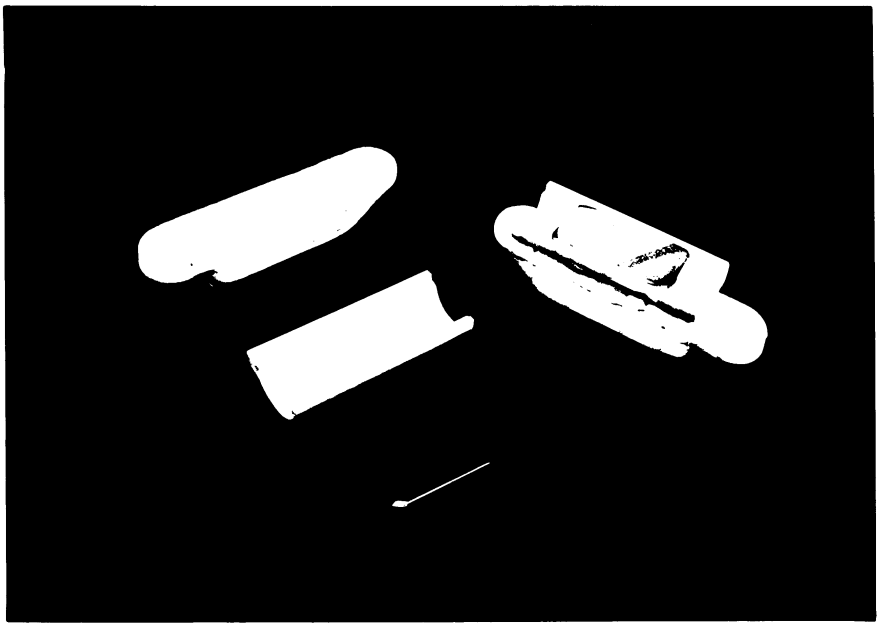

FIG. 1 - SPECIMENS AND HOLDERS.

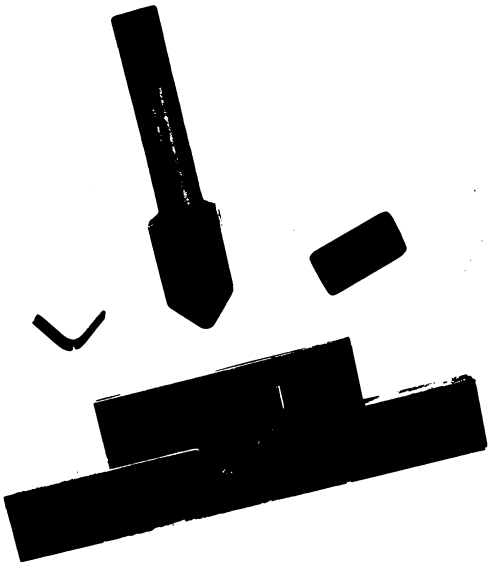

FIG. 2 - BENDING DIE AND SPECIMENS.

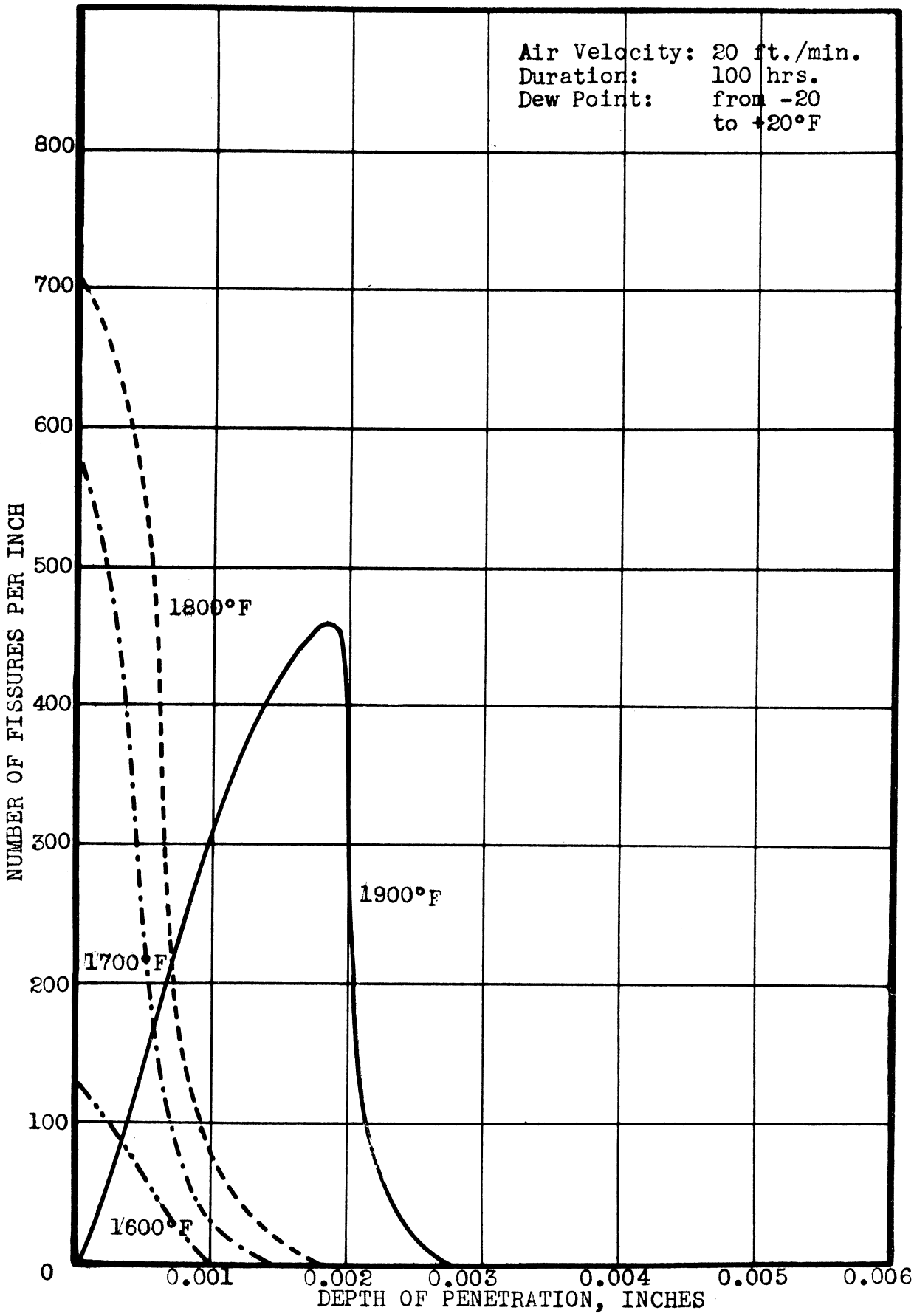

FIG. 3 - PENETRATION CURVES FOR TYPE 309 + Nb ALLOY. RUN 6.

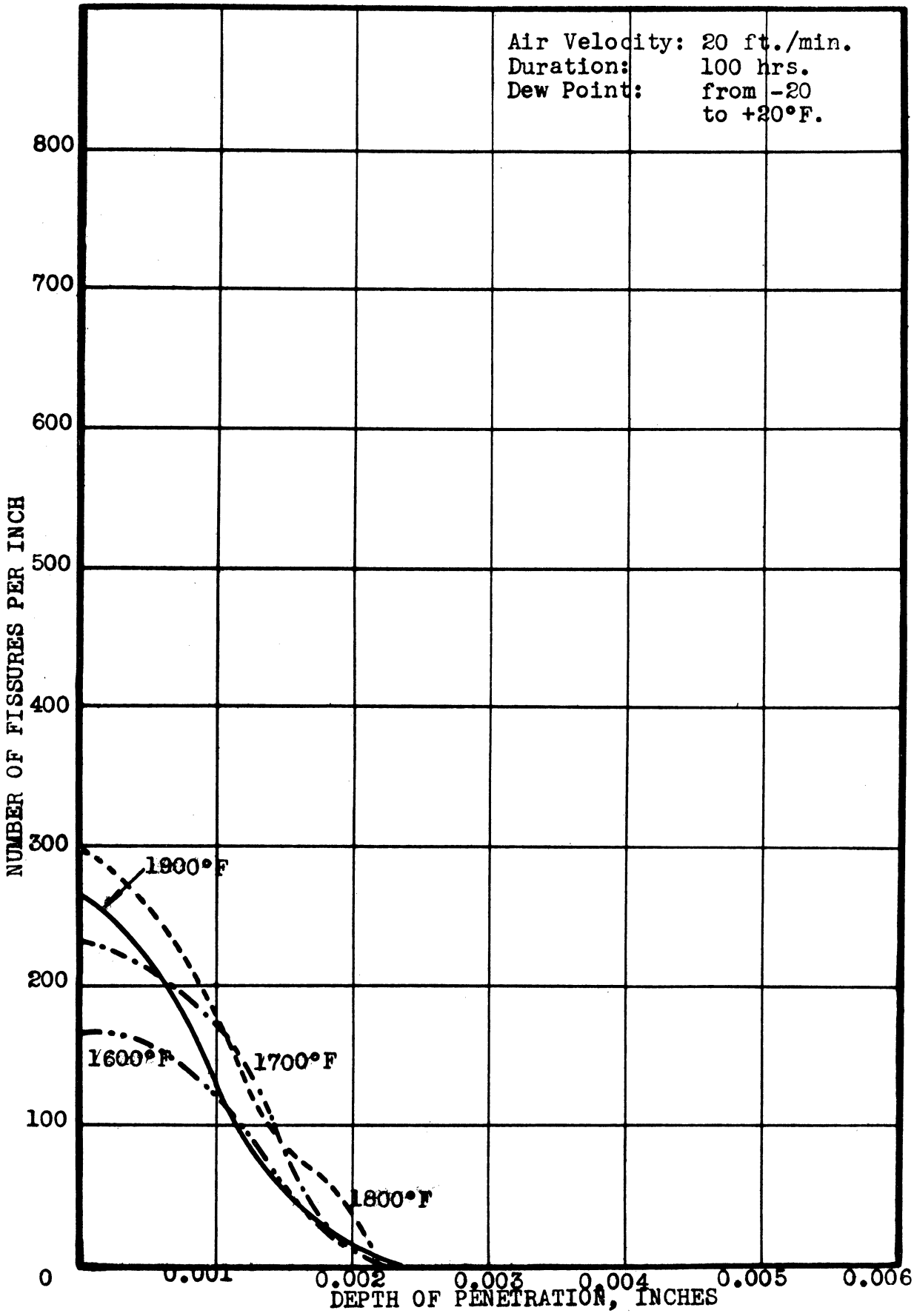

FIG. 4 - PENETRATION CURVES FOR TYPE 310 ALLOY FROM HEAT 64177. RUN 6.

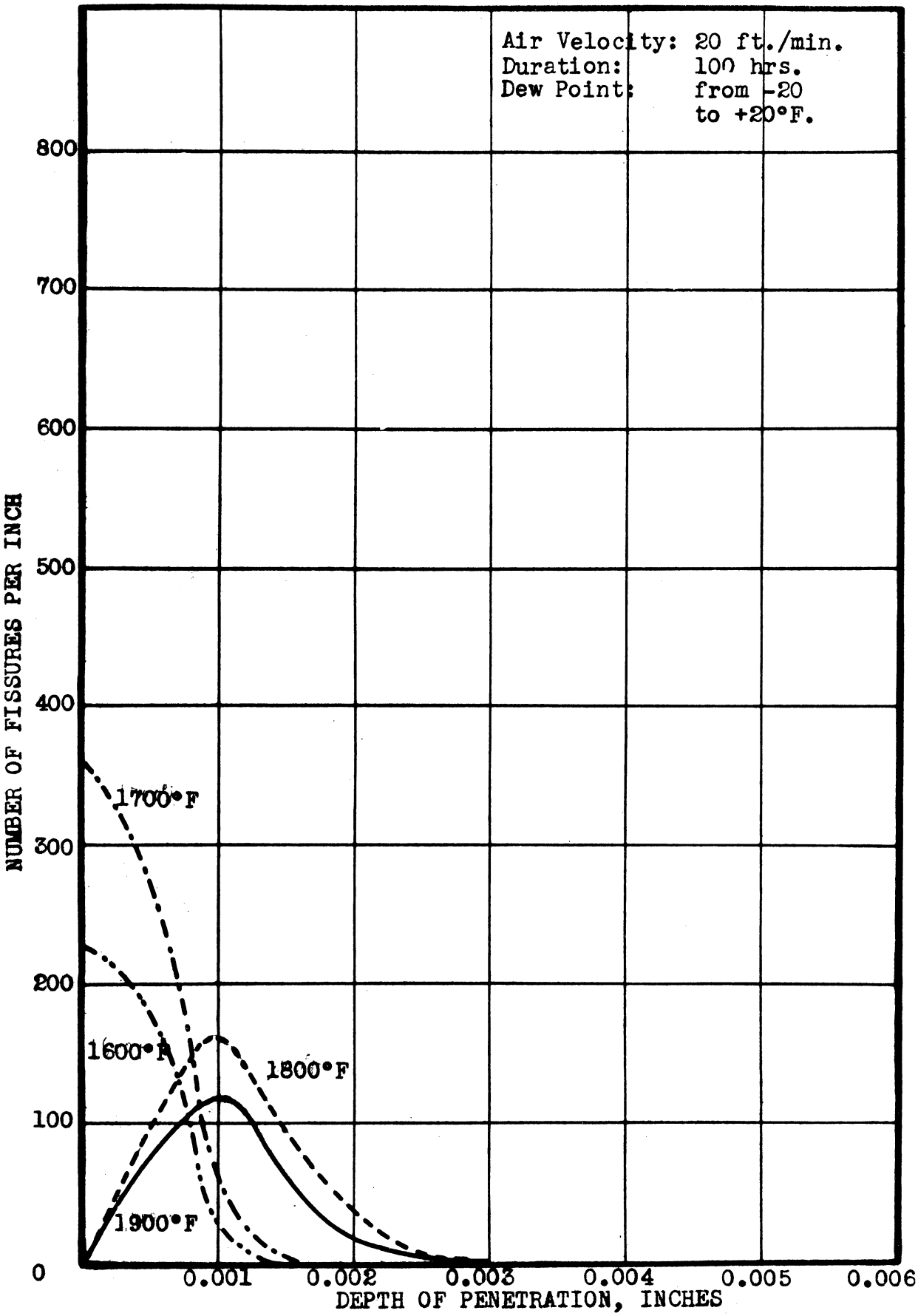

FIG. 5 - PENETRATION CURVES FOR TYPE 310 ALLOY FROM HEAT 64270. RUN 6.

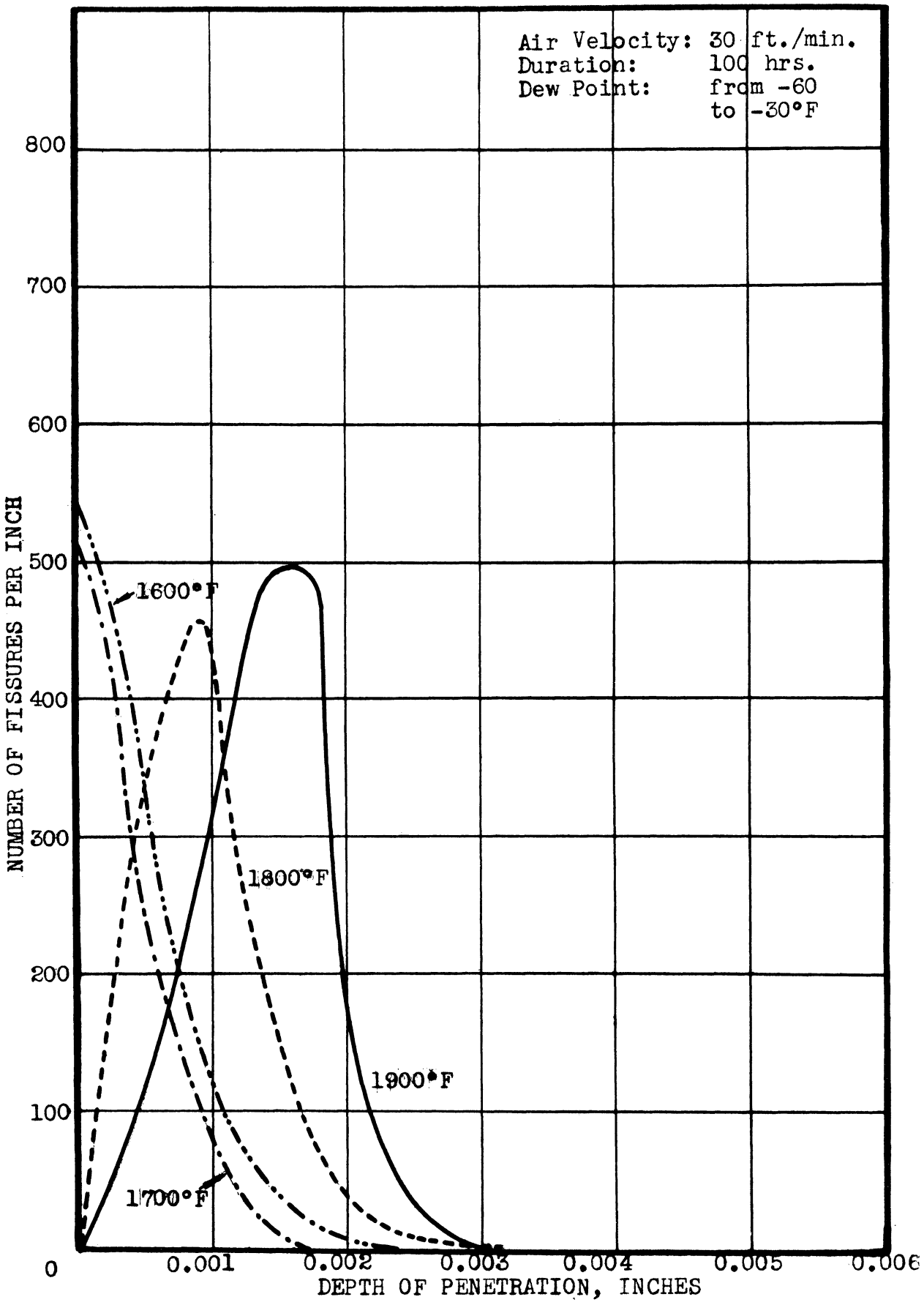

FIG. 6 - PENETRATION CURVES FOR TYPE 309 + Nb ALLOY. RUN 9. STRAIGHT SECTION.

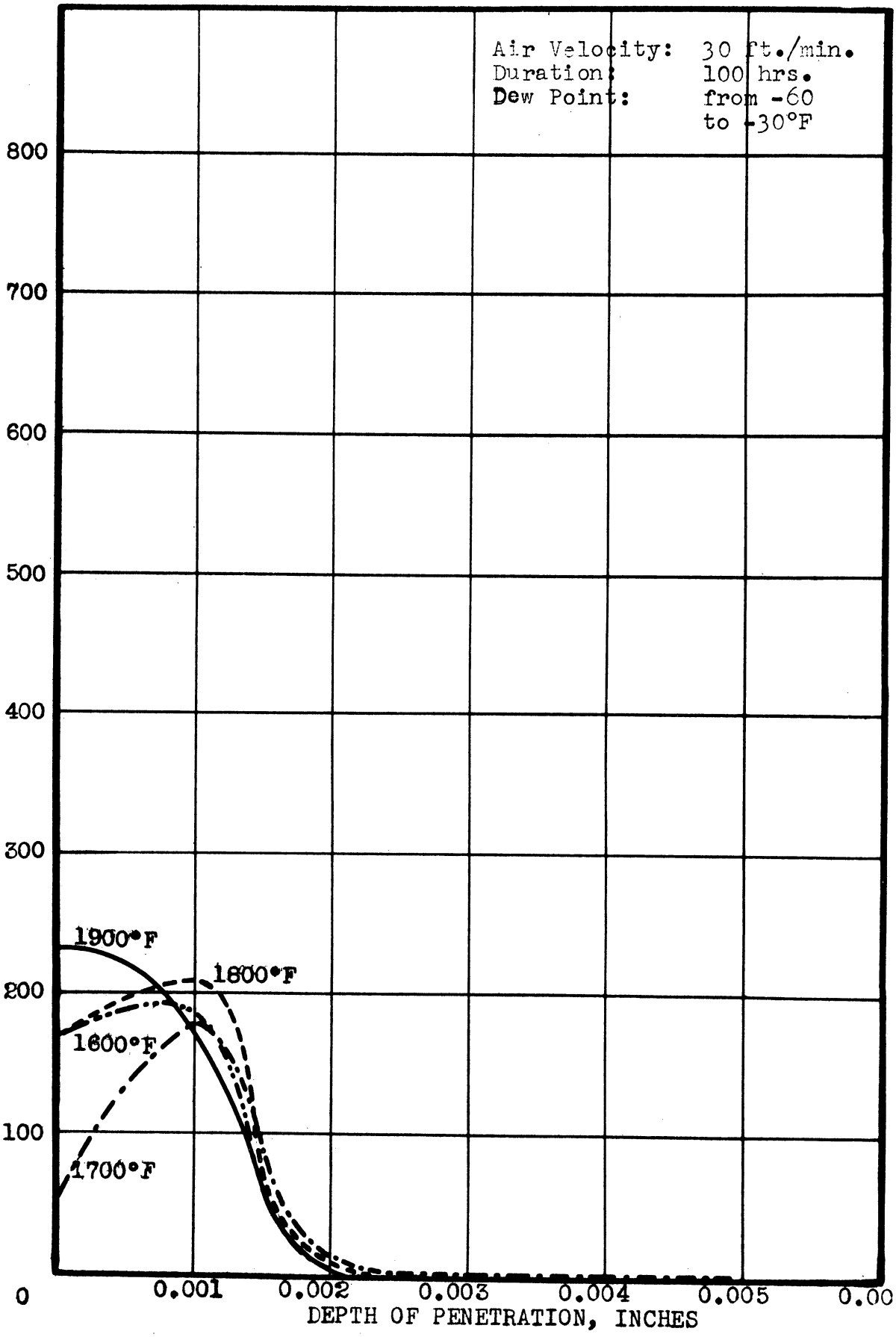

FIG. 7 - PENETRATION CURVES FOR TYPE 310 ALLOY FROM HEAT 64177. RUN 9. STRAIGHT SECTION.

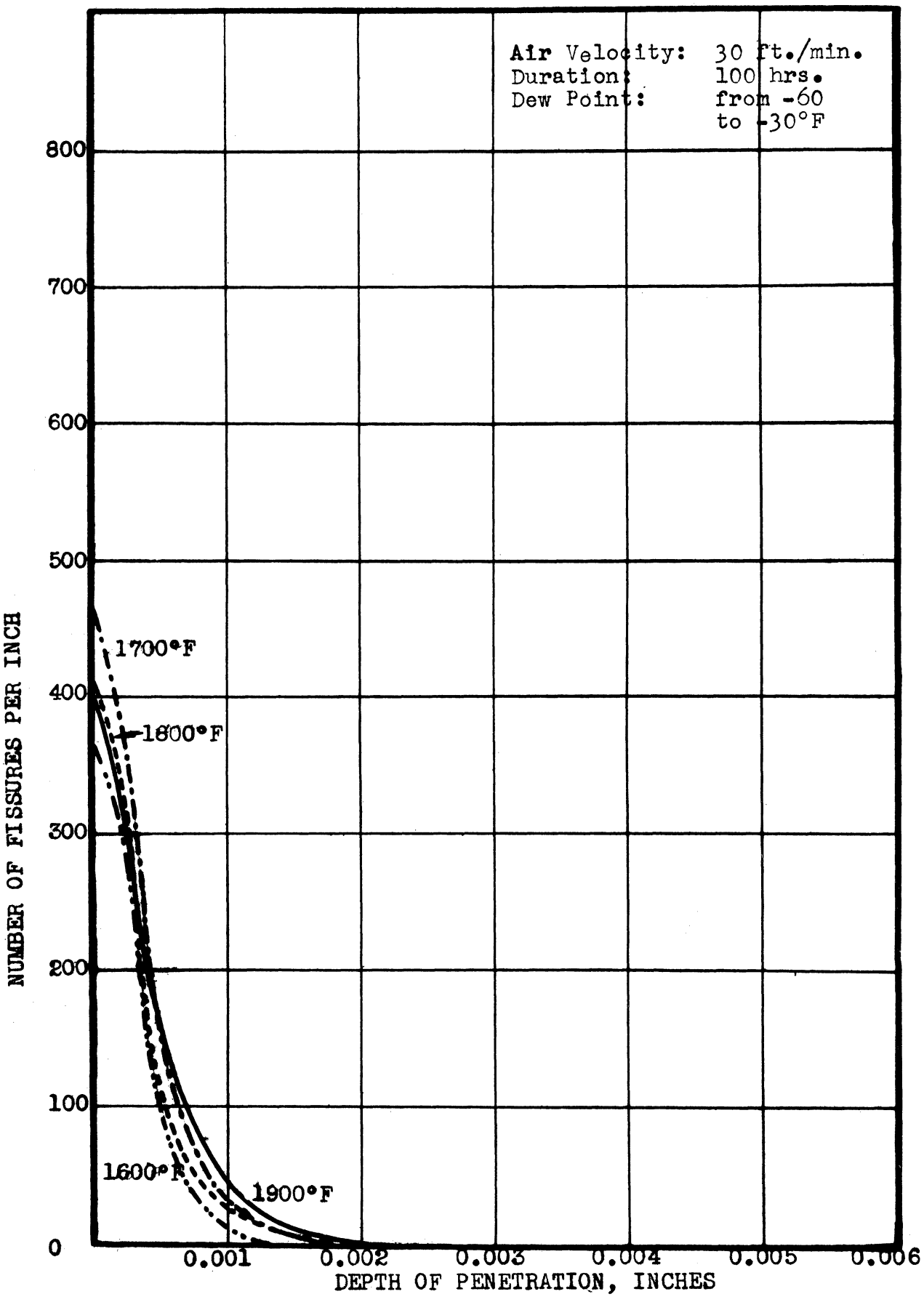

FIG. 8 - PENETRATION CURVES FOR TYPE 310 ALLOY FROM HEAT 64270. RUN 9. STRAIGHT SECTION.

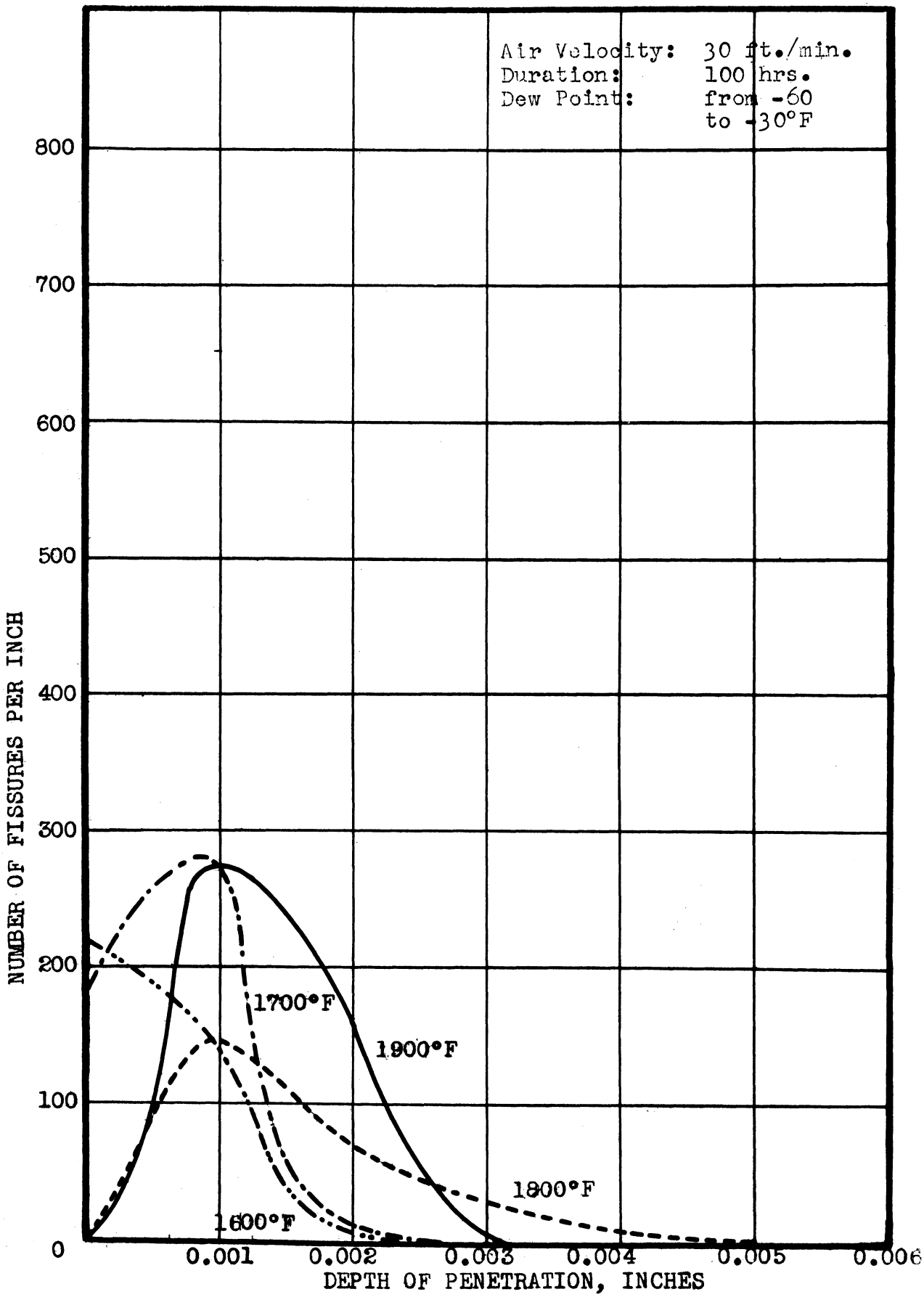

FIG. 9 - PENETRATION CURVES FOR TYPE 309 + Nb ALLOY. RUN 9. CURVED SECTION.

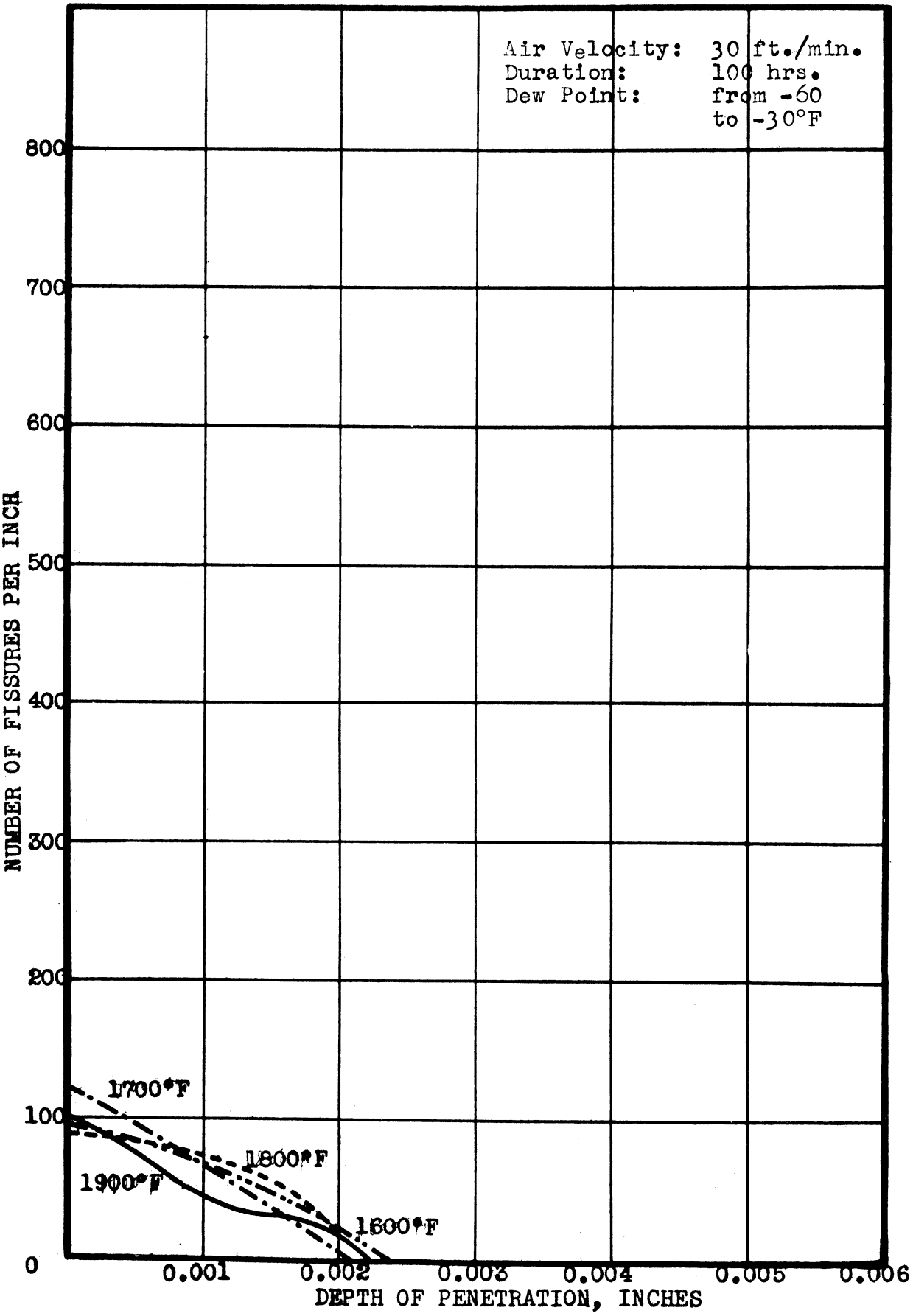

FIG. 10 - PENETRATION CURVES FOR TYPE 310 ALLOY FROM HEAT 64177. RUN 9. CURVED SECTION.

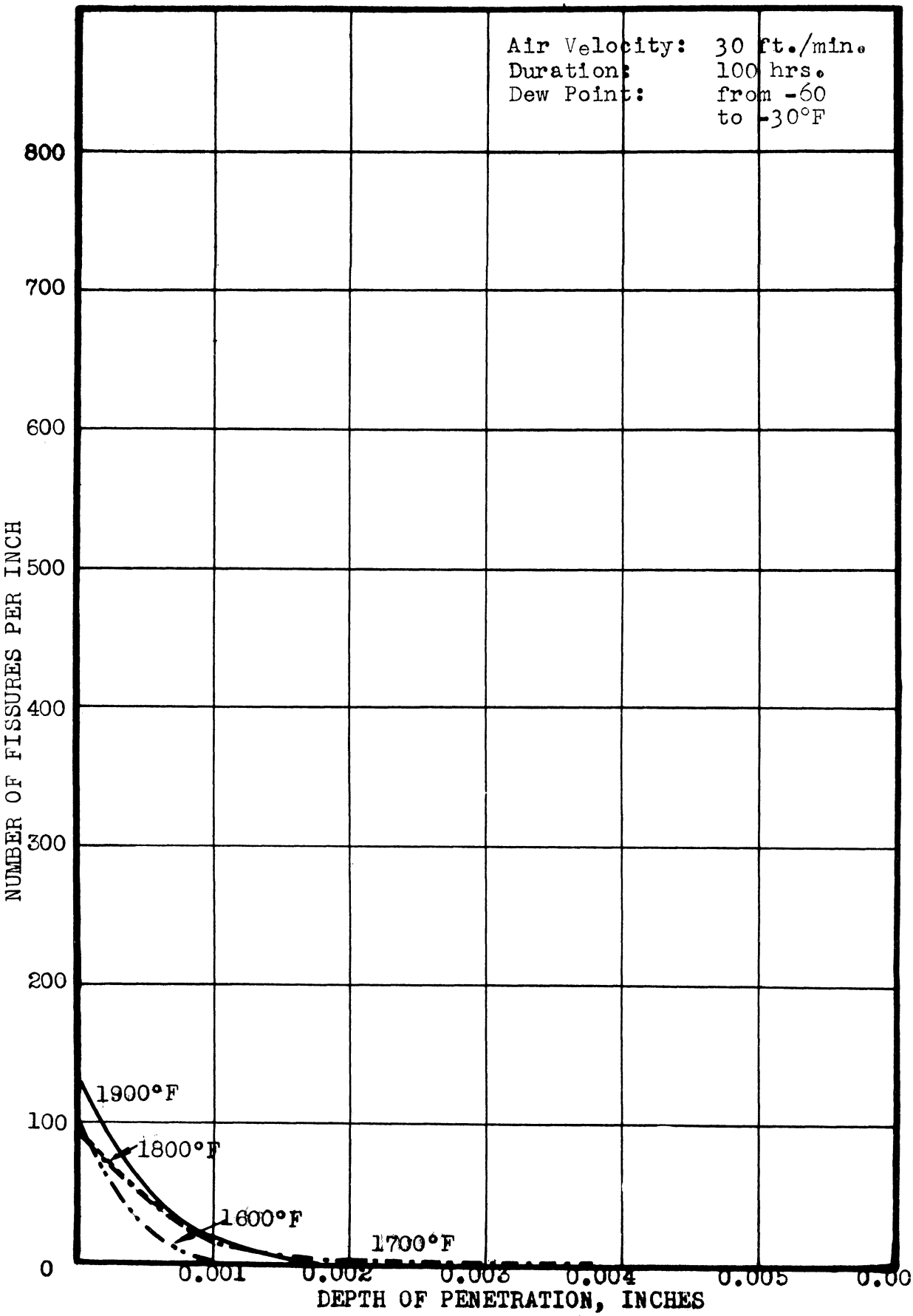

FIG. 11 - PENETRATION CURVES FOR TYPE 310 ALLOY FROM HEAT 64270. RUN 9. CURVED SECTION.

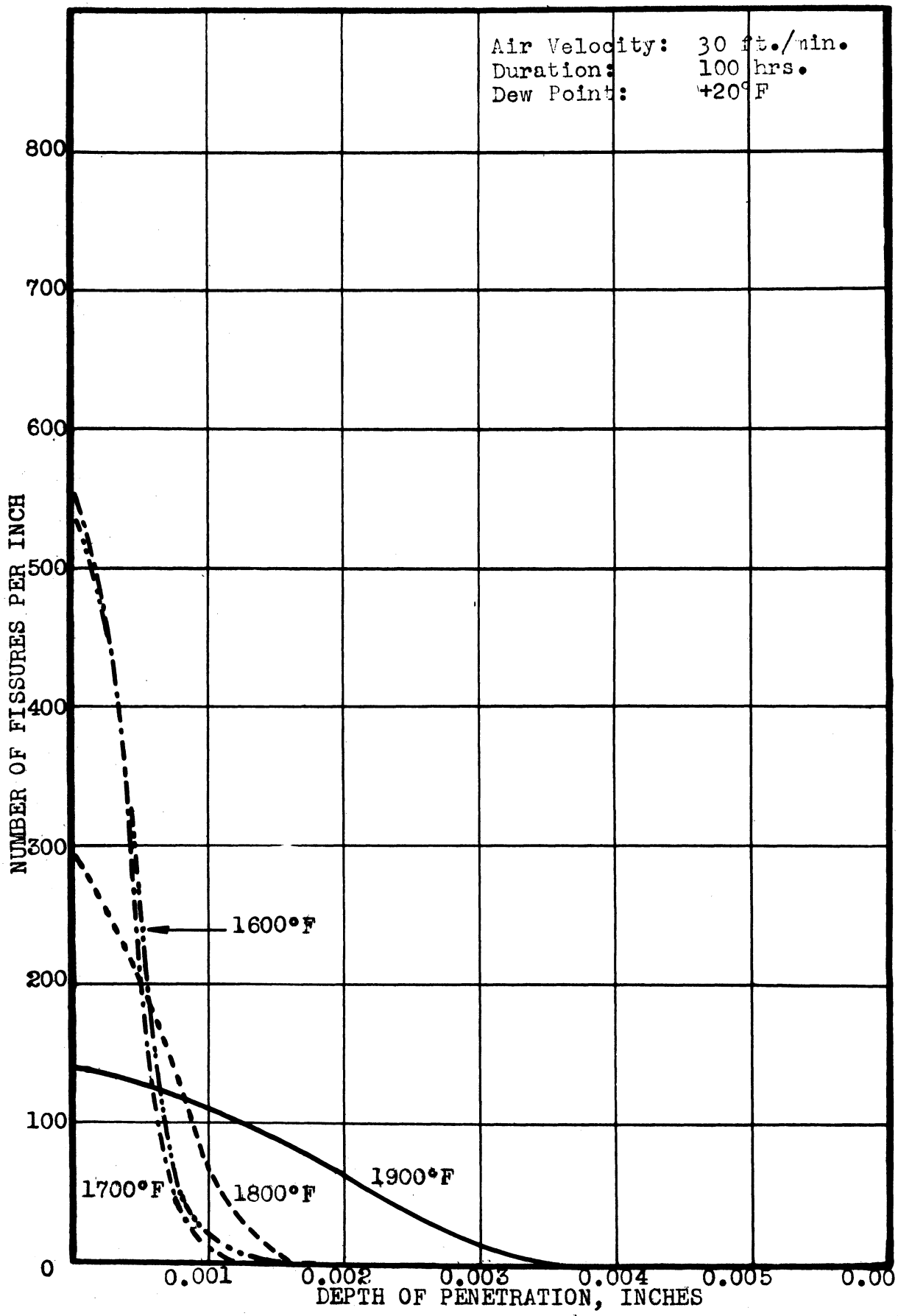

FIG. 12 - PENETRATION CURVES FOR TYPE 309 + Nb ALLOY. RUN 8.

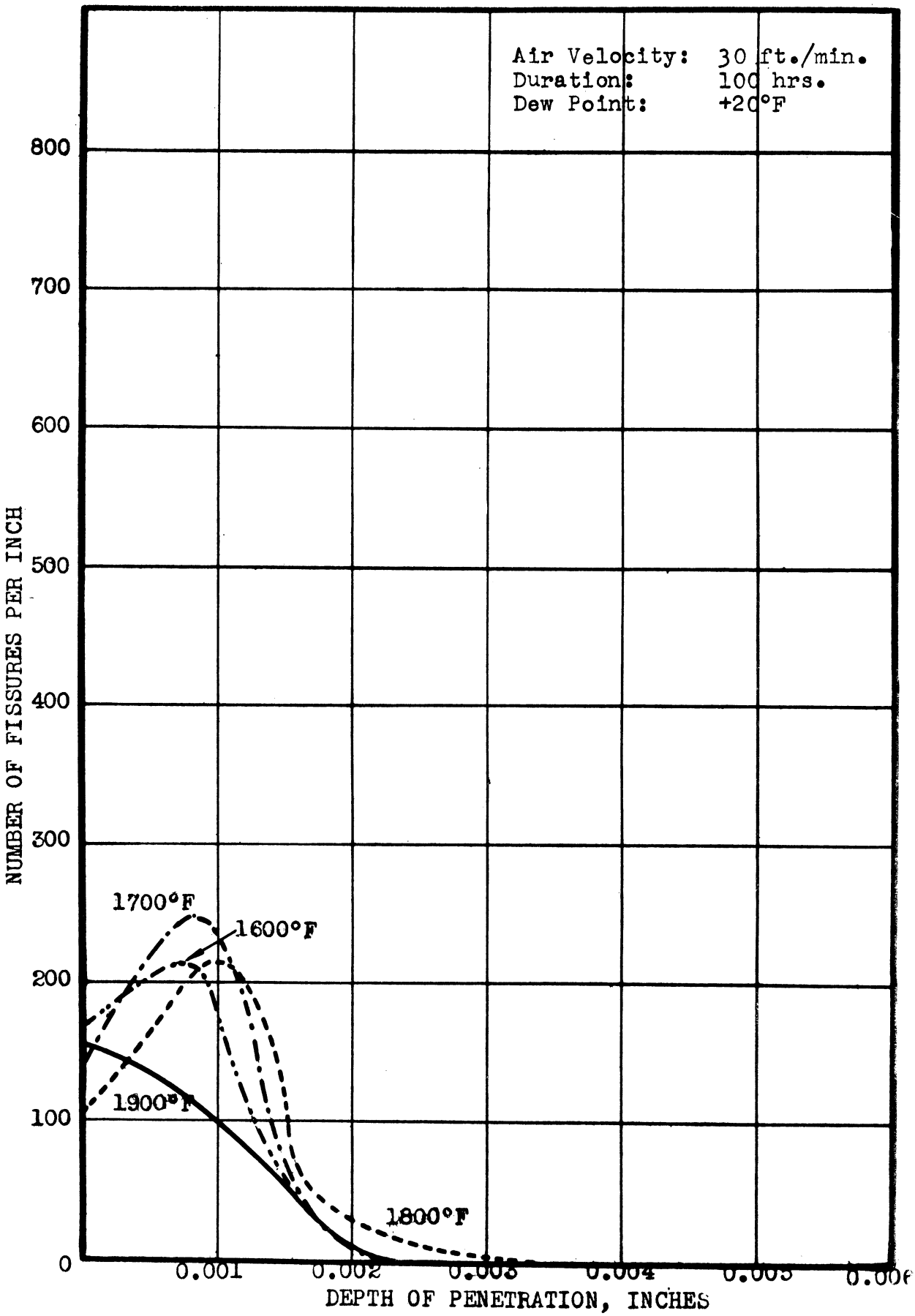

FIG. 13 - PENETRATION CURVES FOR TYPE 310 ALLOY FROM HEAT 64177. RUN 8.

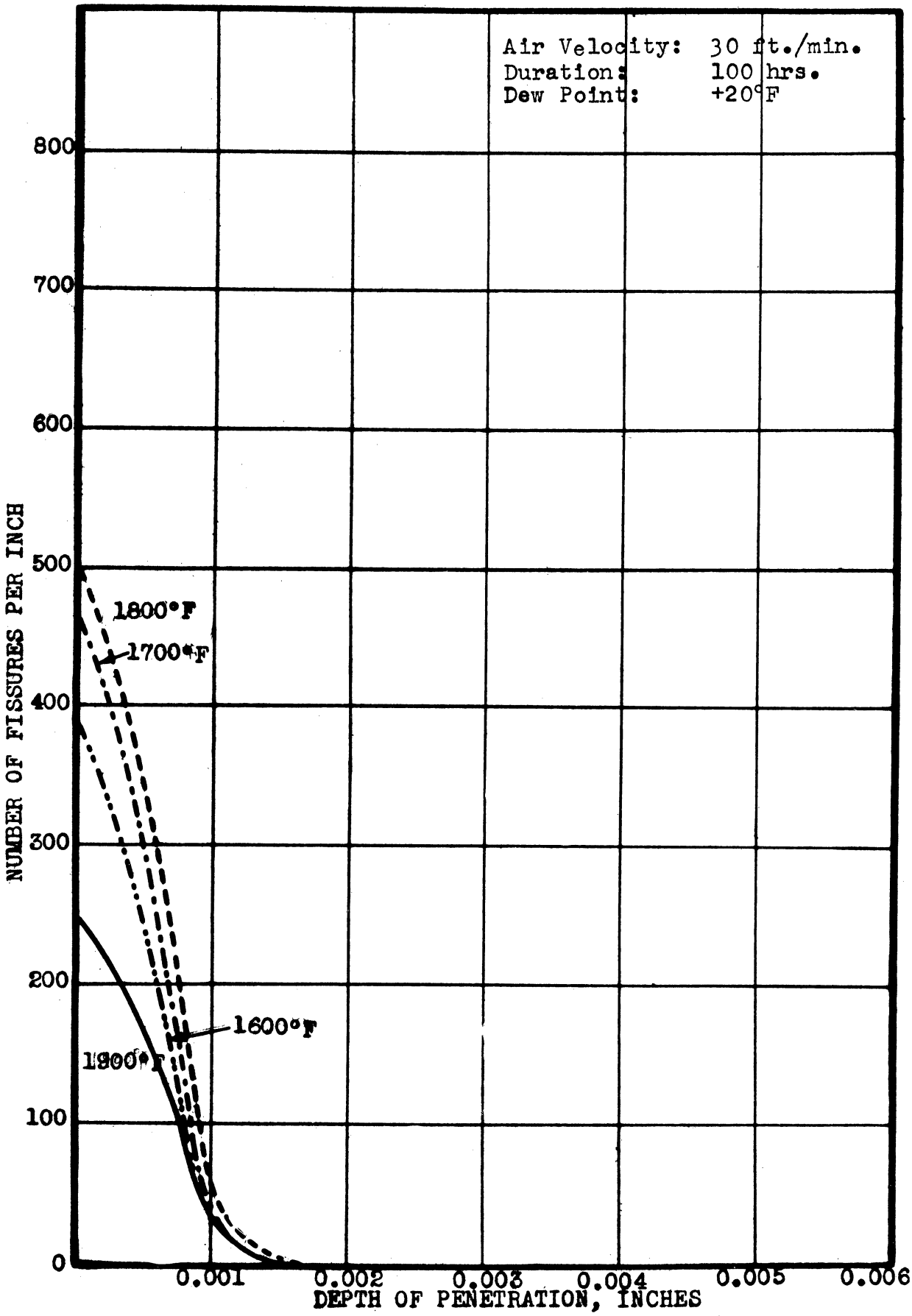

FIG. 14 - PENETRATION CURVES FOR TYPE 310 ALLOY FROM HEAT 64270. RUN 8.

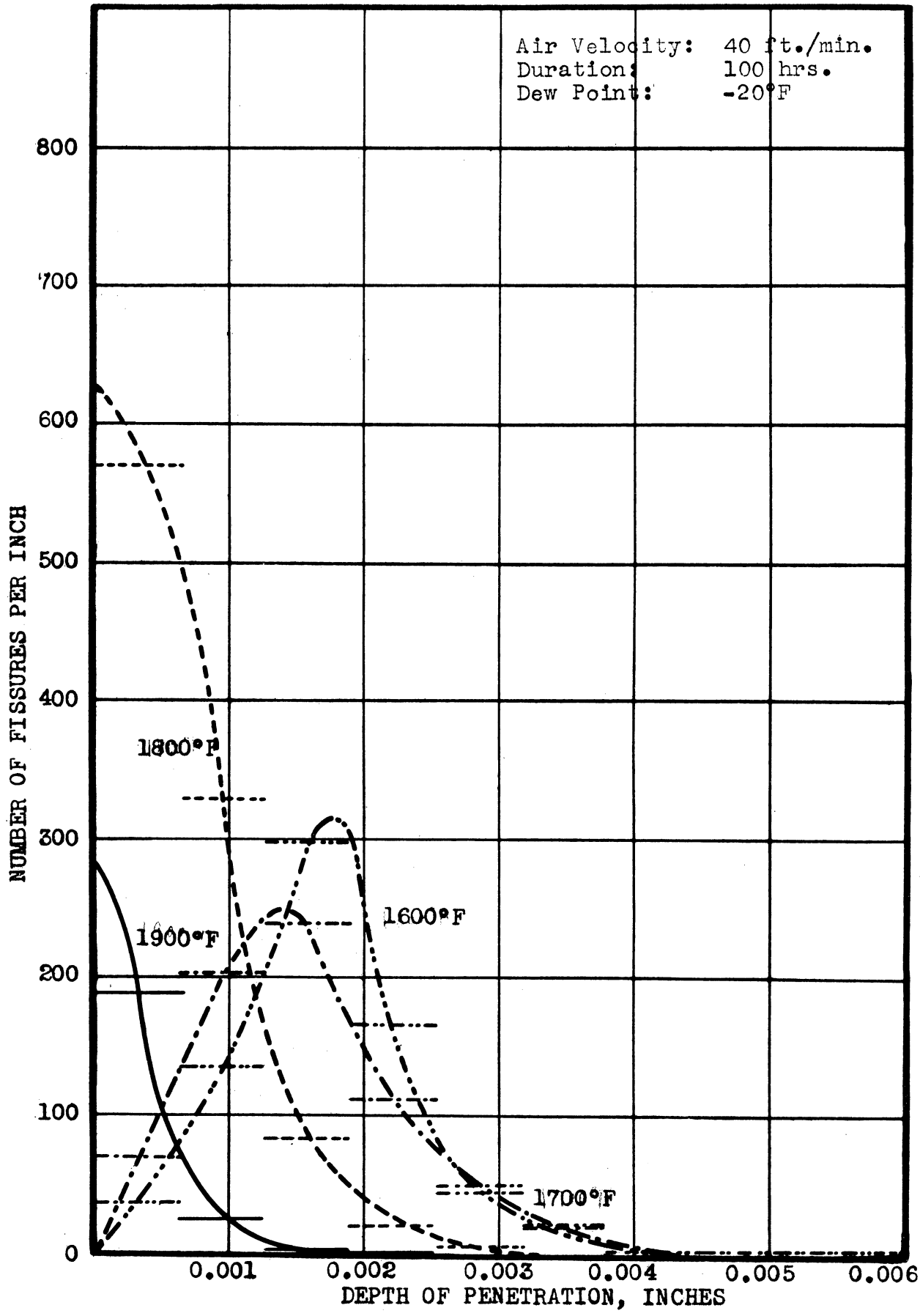

FIG. 15 - PENETRATION CURVES FOR TYPE 309 + Nb ALLOY. RUN 5.

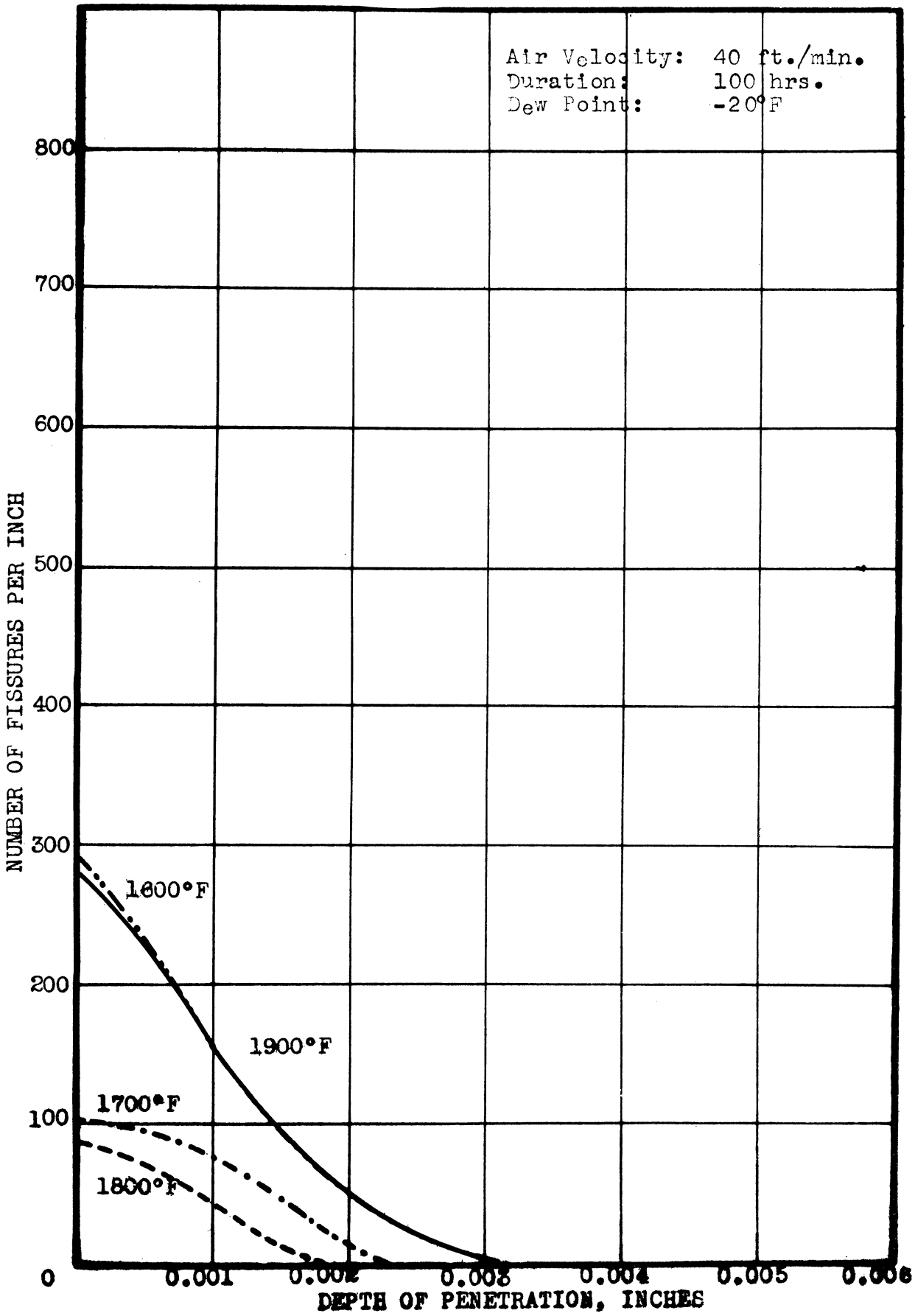

FIG. 16 - PENETRATION CURVES FOR TYPE 310 ALLOY FROM HEAT 64177. RUN 5.

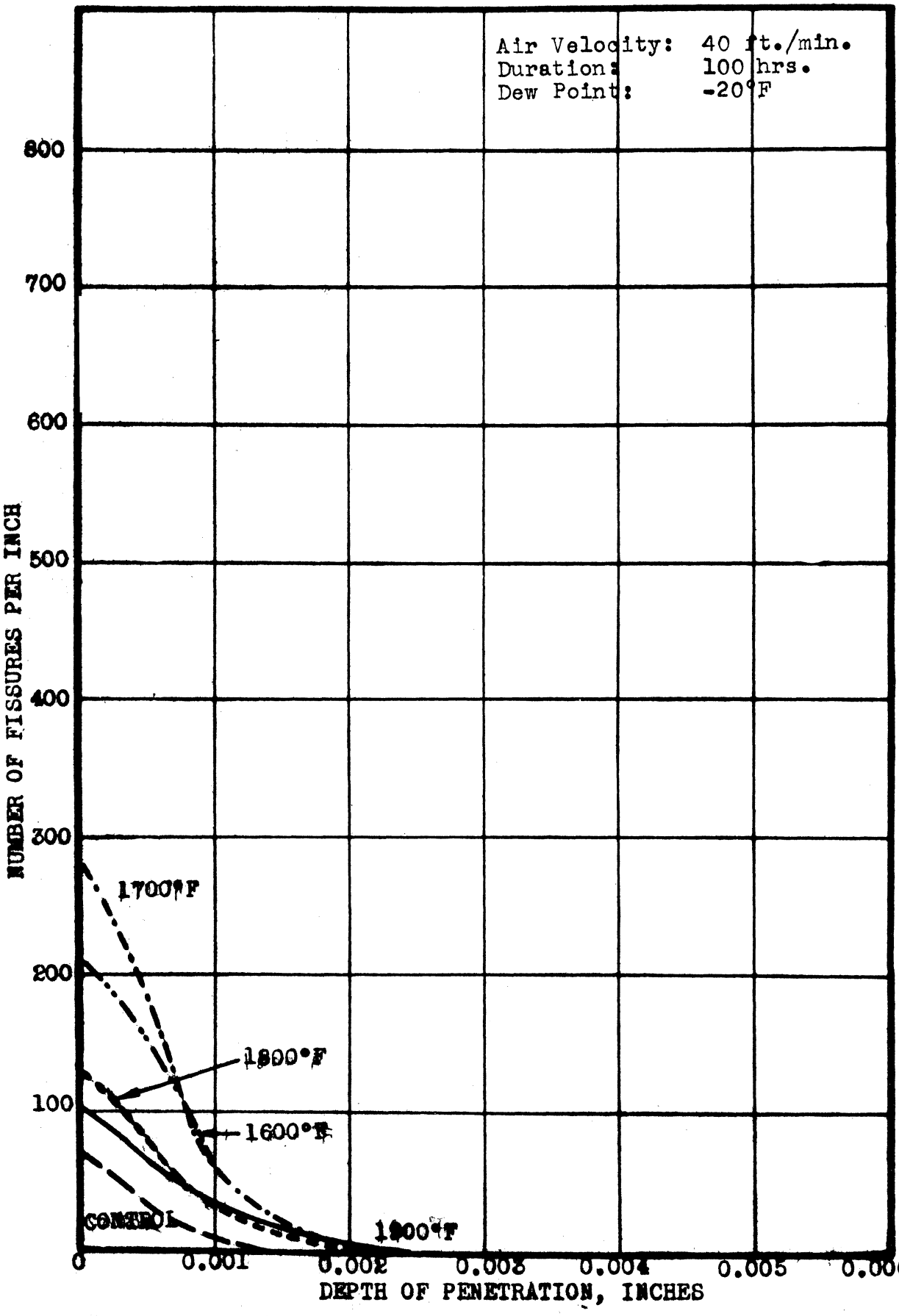

FIG. 17 - PENETRATION CURVES FOR TYPE 310 ALLOY FROM HEAT 64270. RUN 5.

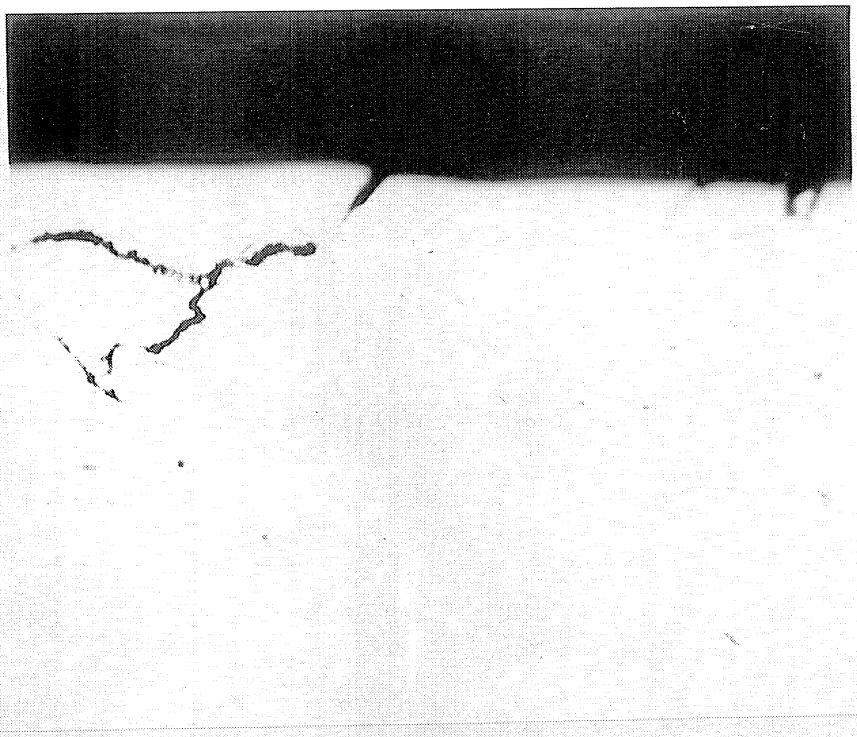

(a)
1000 X

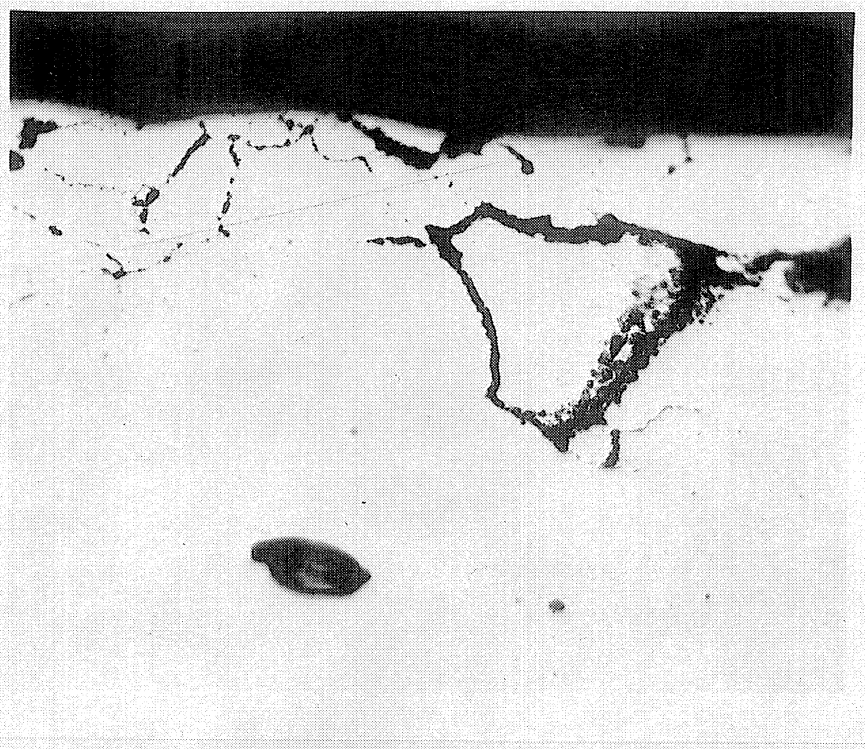

(b)
1000 X

FIG. 18 - TYPICAL MICROSTRUCTURES OF TYPE 310 ALLOY FROM HEAT 64177. UNETCHED.

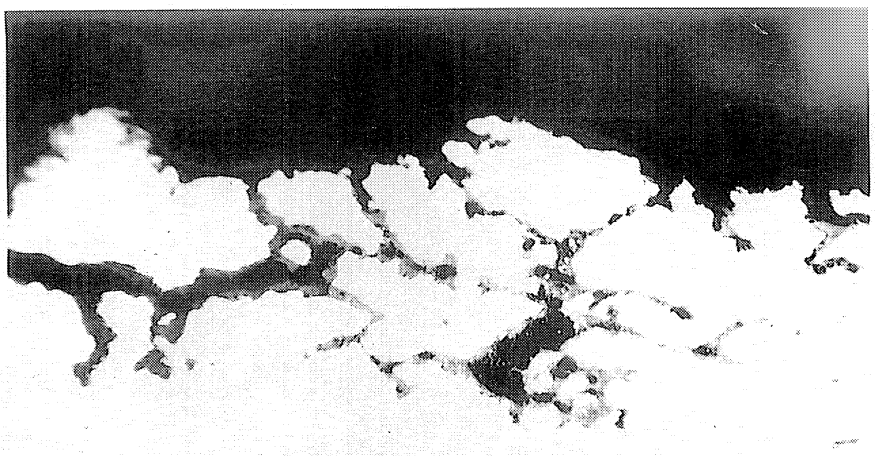

(a)
1000 X

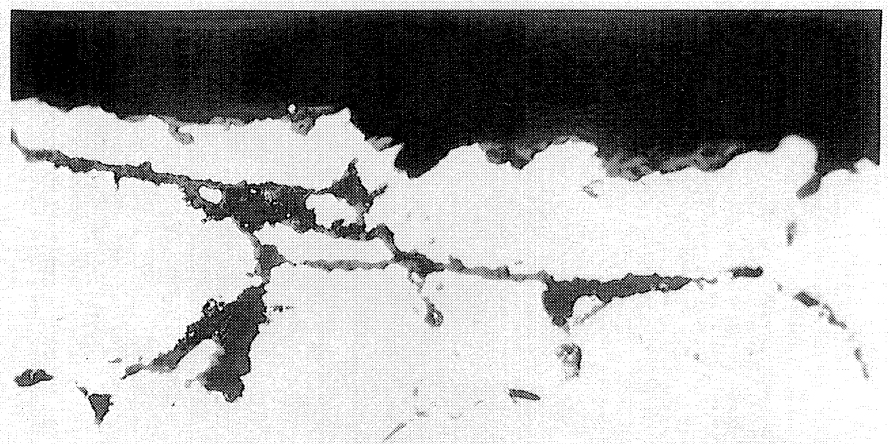

(b)
1000 X

FIG. 19 - MICROSTRUCTURES OF TYPE 310 ALLOY FROM HEAT 64177 AFTER OXIDATION. RUN 6. UNETCHED.

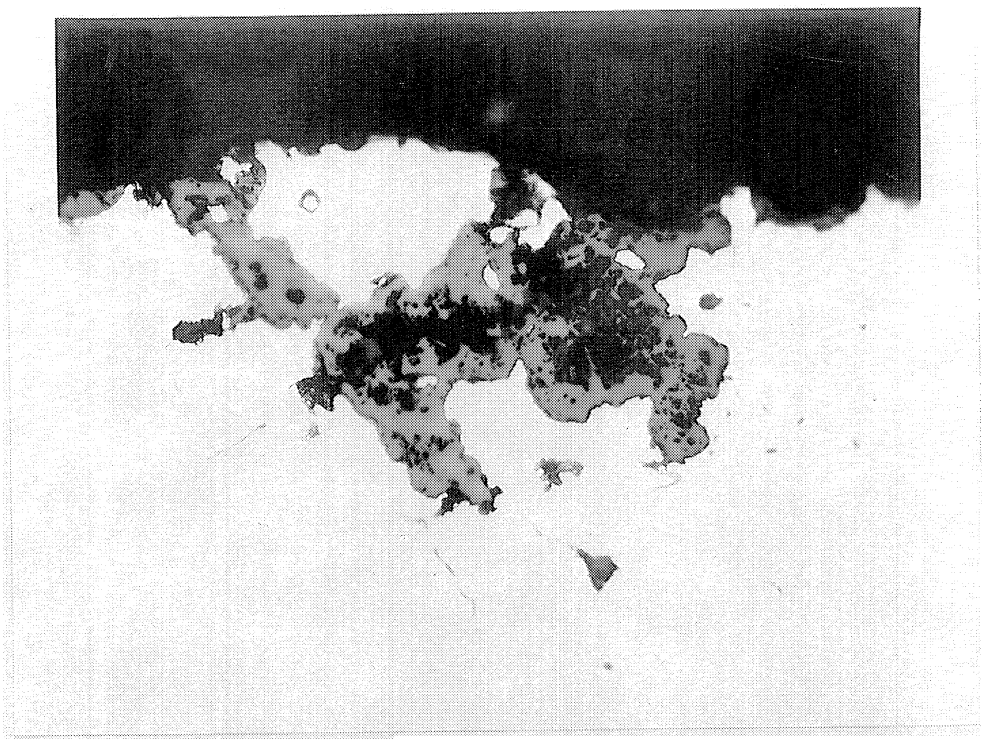

(c)
1000 X

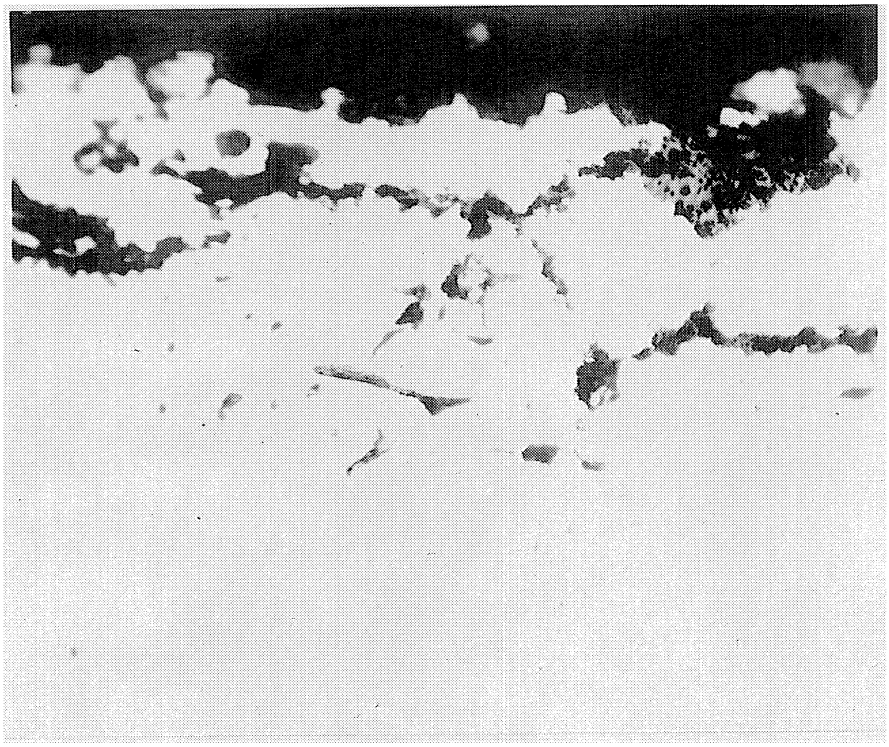

(d)
1000 X

FIG. 19 (CONT'D.) - MICROSTRUCTURES OF TYPE 310 ALLOY FROM HEAT 64177 AFTER OXIDATION. RUN 6. UNETCHED.

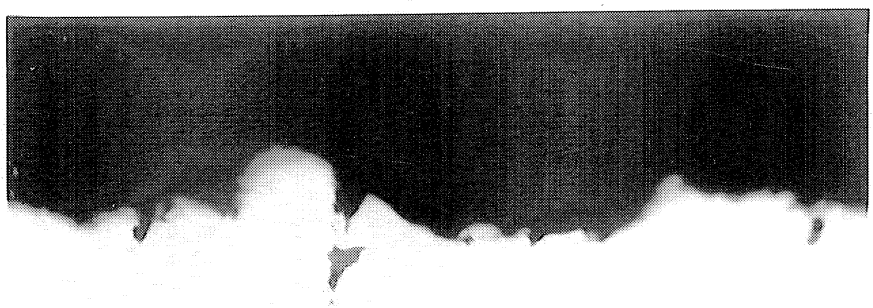

(a)
1000 X

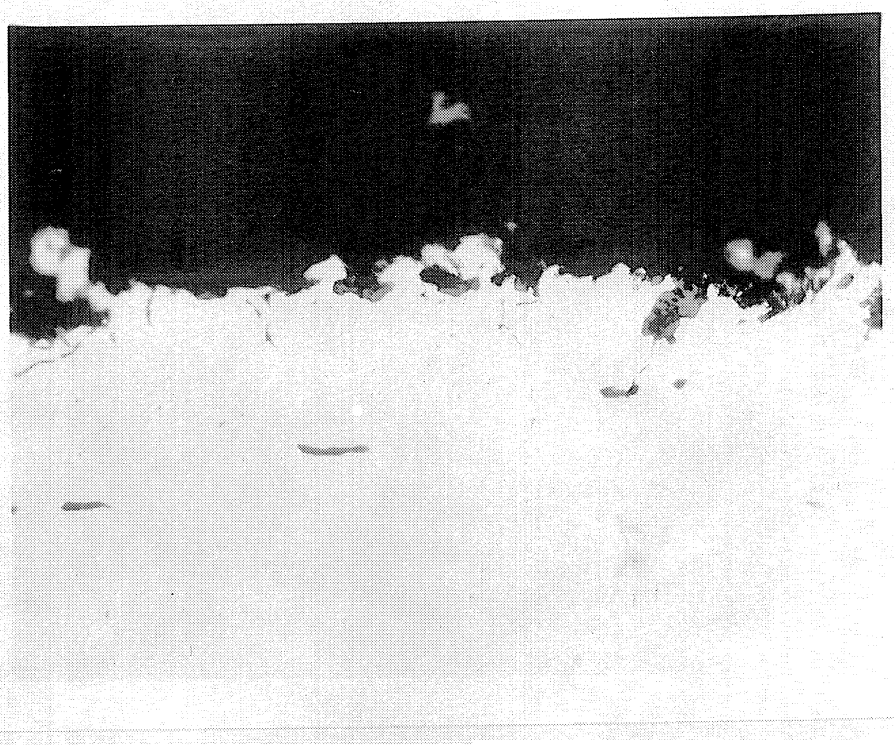

(b)
1000 X

FIG. 20 - MICROSTRUCTURES OF TYPE 310 ALLOY FROM HEAT 64270 AFTER OXIDATION. RUN 6. UNETCHED.

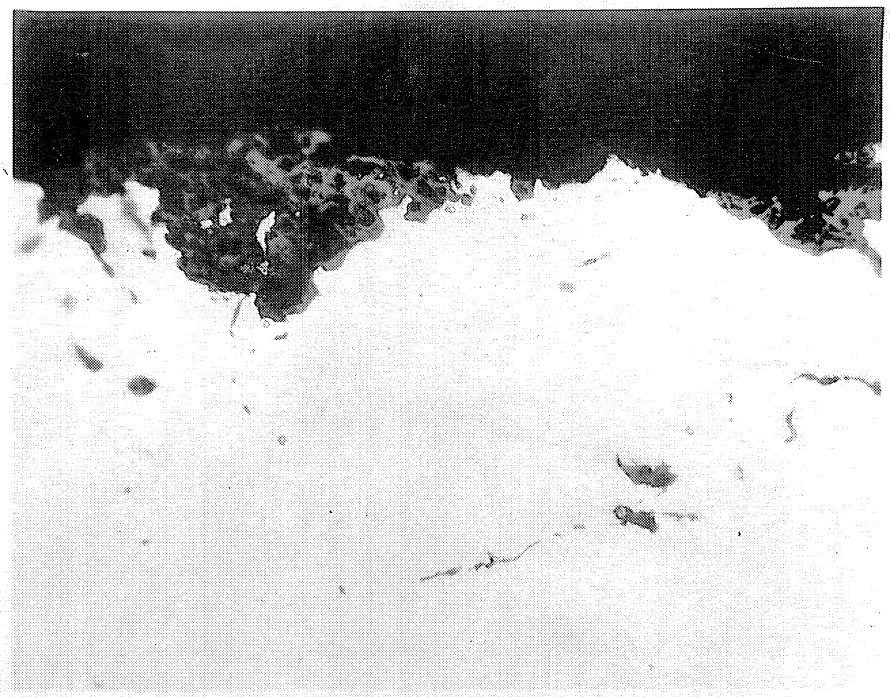

(c)
1000 X

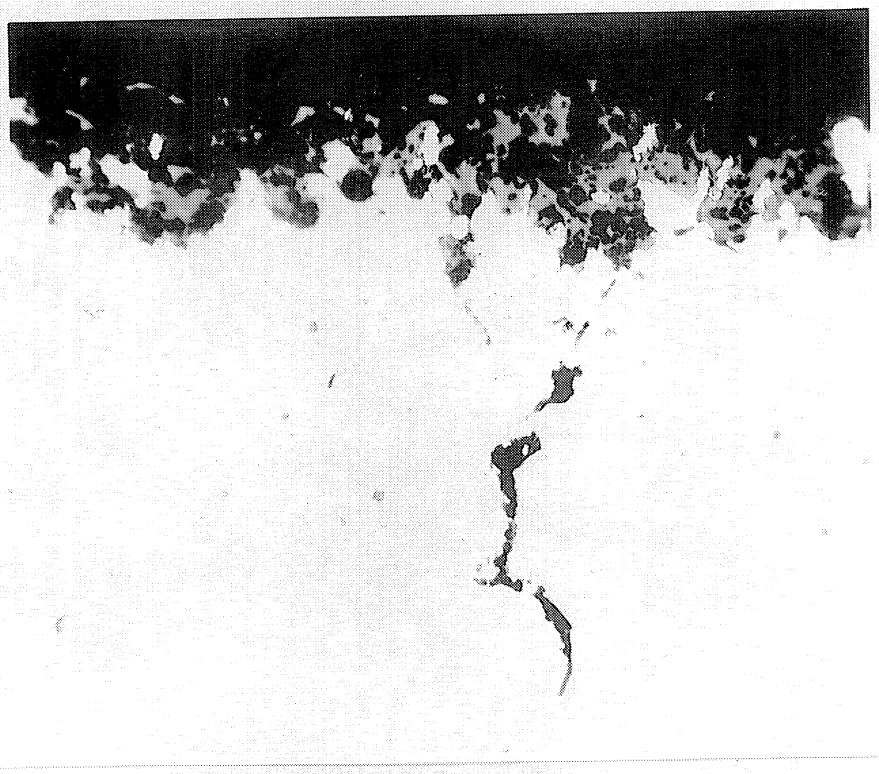

(d)
1000 X

FIG. 20 (CONT'D.) - MICROSTRUCTURES OF TYPE 310 ALLOY FROM HEAT 64270 AFTER OXIDATION. RUN 6. UNETCHED.

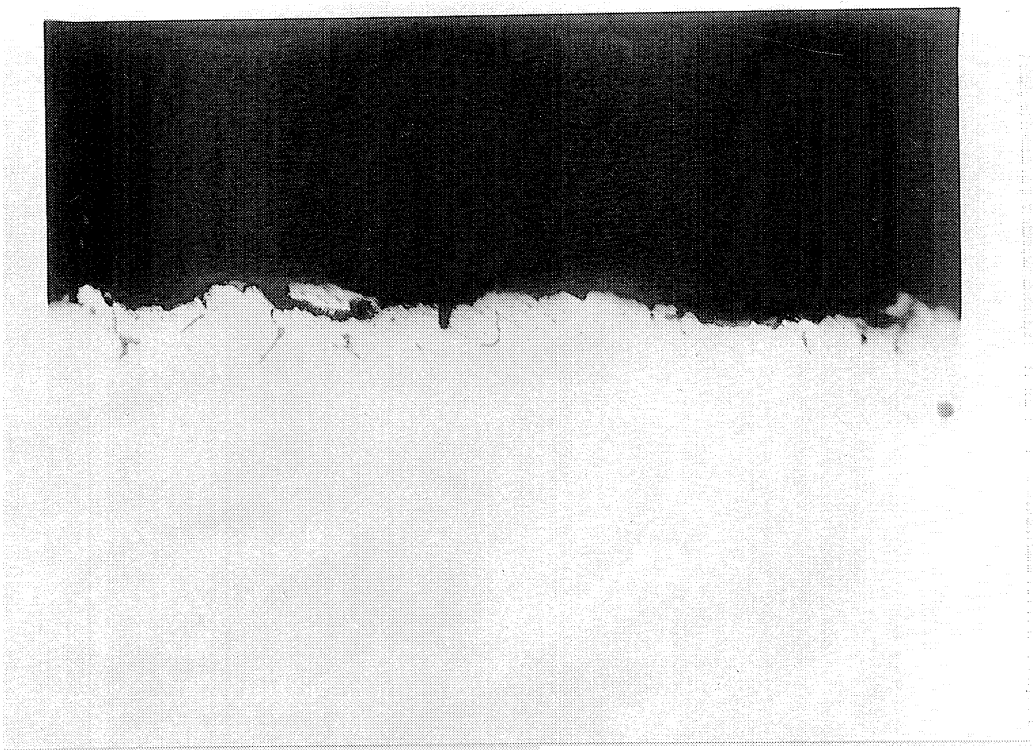

(a)
1000 X

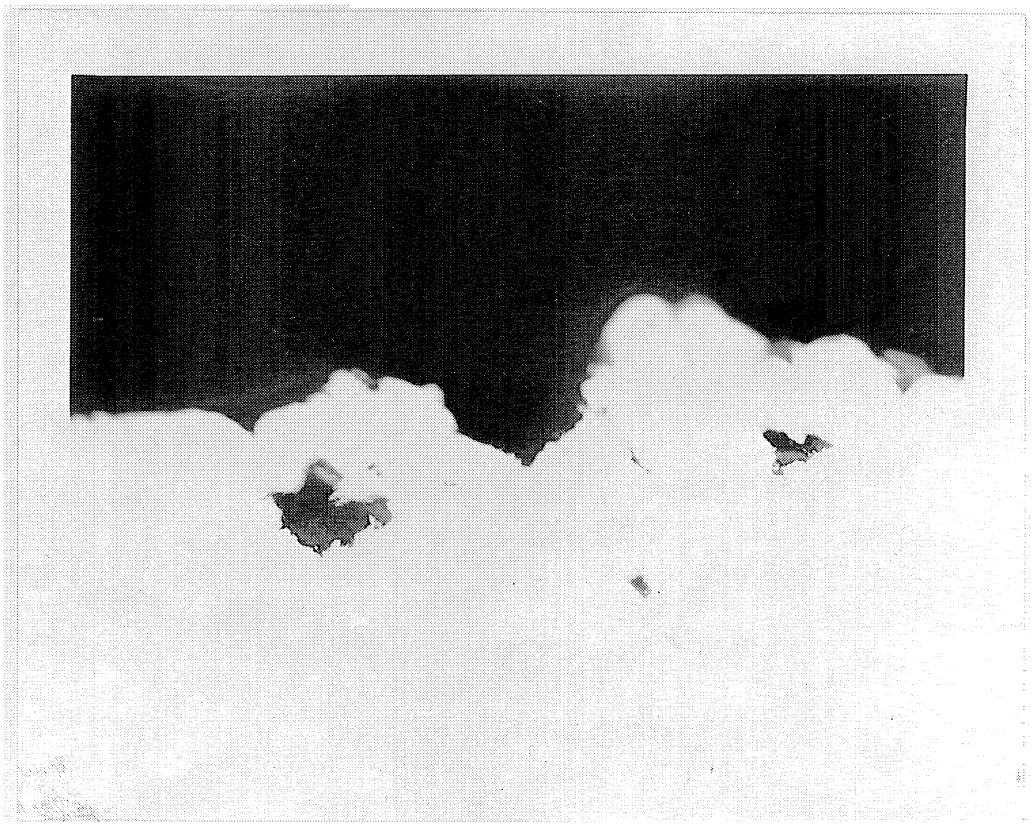

(b)
1000 X

FIG. 21 - MICROSTRUCTURES OF TYPE 309 + Nb ALLOY AFTER OXIDATION. RUN 9. UNETCHED.

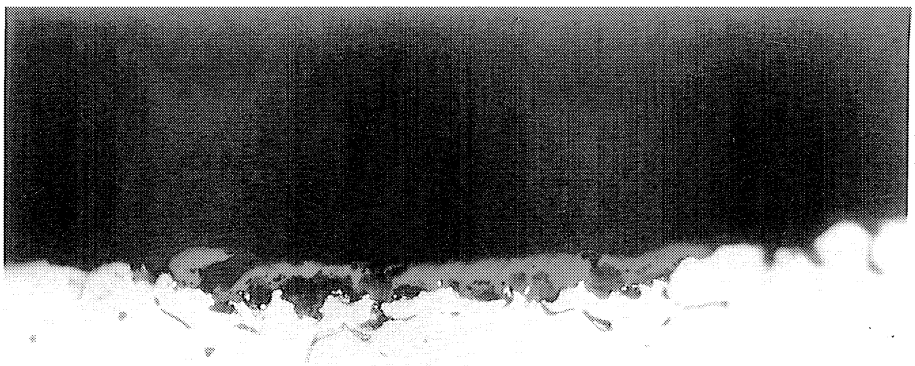

(c)
1000 X

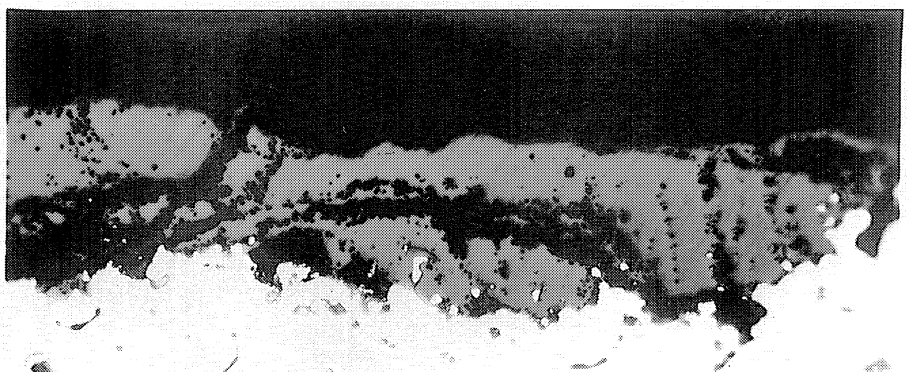

(d)
1000 X

FIG. 21 (CONT'D.) - MICROSTRUCTURES OF TYPE 309 + Nb ALLOY AFTER OXIDATION. RUN 9. UNETCHED.

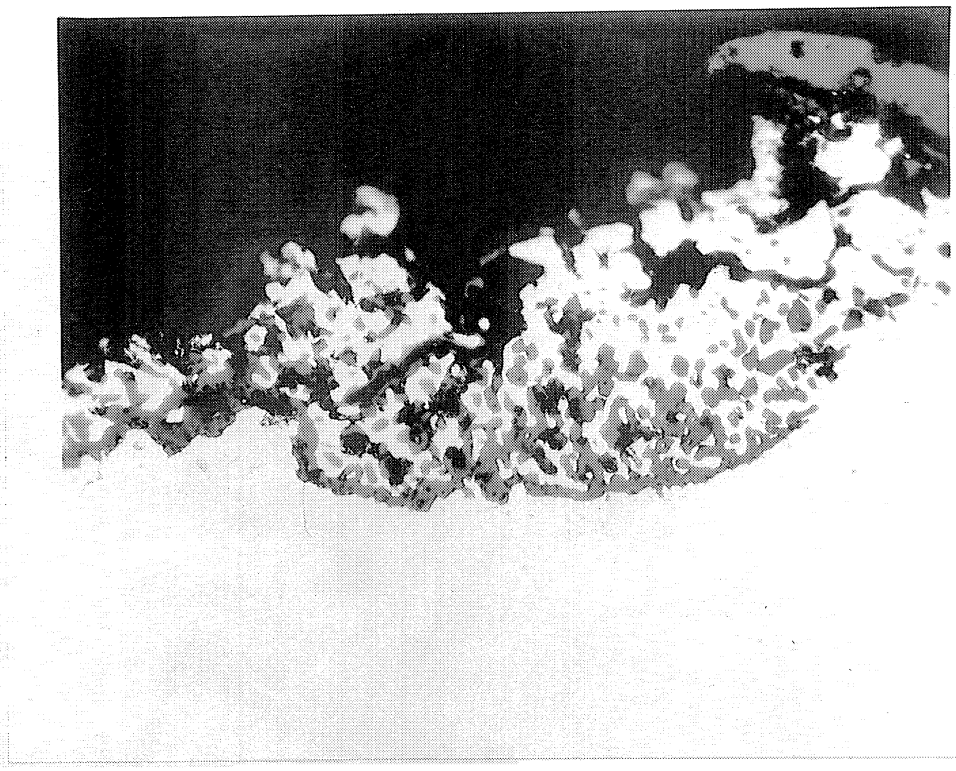

1000 X

FIG. 22 - ATYPICAL MICROSTRUCTURE OF TYPE 309 + Nb ALLOY AT 1900°F. RUN 9. UNETCHED.

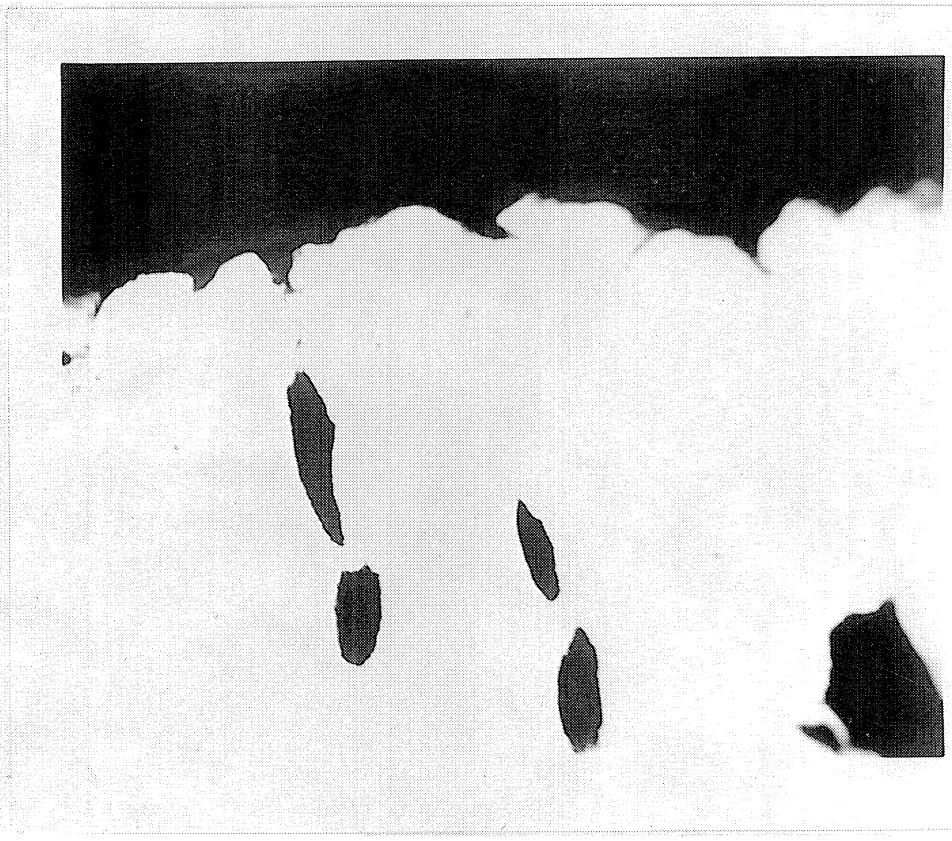

1000 X

FIG. 23 - ATYPICAL MICROSTRUCTURE OF TYPE 309 + Nb ALLOY AT 1900°F. RUN 8. UNETCHED.

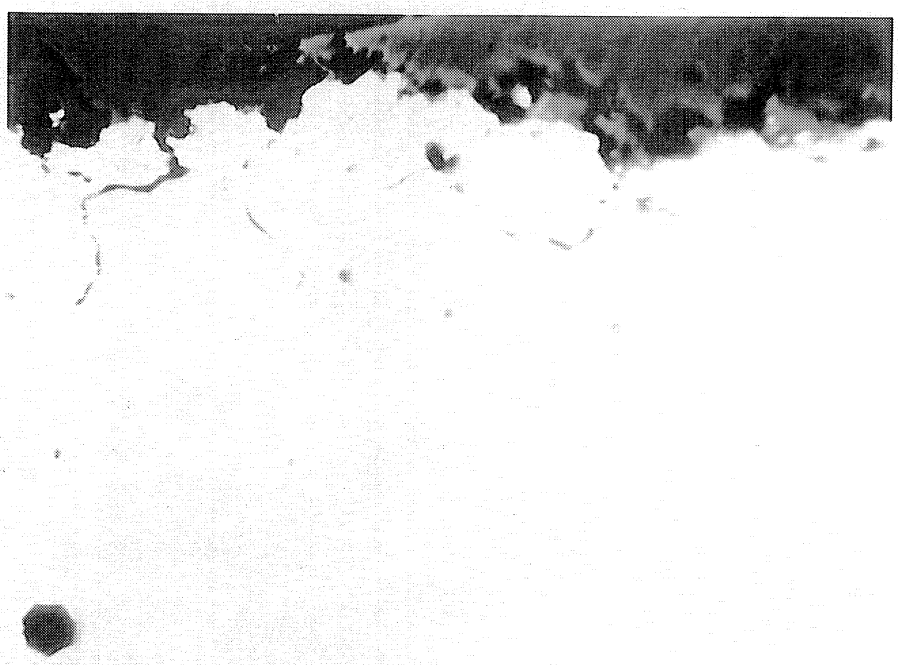

1000 X

FIG. 24 - MICROSTRUCTURE OF TYPE 309 + Nb ALLOY AT 1900°F SHOWING ANGULAR INCLUSION. RUN 9. UNETCHED.